NOVA SCHOOL OF SCIENCE & TECHNOLOGY

DEPARTAMENT OF MATERIALS SCIENCE

CAROLINA SILVESTRE CARNEIRO PEREIRA

BSc in Materials Engineering

NATURE DERIVED FUNCTIONAL MATERIALS FOR SMART PACKAGING

MASTER IN MATERIALS ENGINEERING

NOVA University Lisbon

September, 2024

DEPARTAMENT OF
MATERIALS SCIENCE

NATURE DERIVED FUNCTIONAL MATERIALS FOR SMART PACKAGING

CAROLINA SILVESTRE CARNEIRO PEREIRA

BSc in Materials Engineering

Adviser: Henrique Vazão de Almeida
Junior Reseacher, CENIMAT|i3N, NOVA School of Science and Technology

Co-advisers: Suman Nandy
Principal Researcher, CENIMAT|i3N, NOVA School of Science and Technology

Examination Committee:

Chair: Maria Helena Godinho,
Associate Professor with Habilitation, Material Science Department, NOVA School of Science and Technology

Rapporteur: Diana Gaspar,
Senior Researcher, AlmaScience

Adviser: Henrique Vazão Almeida,
Junior Researcher, CENIMAT|i3N, NOVA School of Science and Technology

MASTER IN MATERIALS ENGINEERING

NOVA University Lisbon
September 2024

Nature Derived Functional Materials for Smart Packaging

This document was created with Microsoft Word text processor and the NOVAthesis Word template [1].

Acknowledgments

I would like to express my deepest gratitude to NOVA School of Science and Technology, particularly the Materials Science Department, for being my home over the past five years. I am immensely grateful to the professors, assistants, researchers, and staff for their valuable lessons and support throughout my journey.

I owe special thanks to my advisors, Henrique Almeida and Suman Nandy, whose guidance, availability, and unwavering support were instrumental in the completion of this work, even when it stretched beyond schedule. I am also thankful to Sumita Goswami for her timely advice on numerous aspects of this research, and to Guilherme Ferreira for helping me navigate the initial stages, offering invaluable tips, and spending long hours in the lab with me, especially during our time with the humidity chamber (gladly it has yet to spontaneously combust).

I would like to thank Rafael Resende for his assistance with SEM, contact angle, and tensile tests, and for his availability despite his busy schedule. I'm grateful to Prof. Ricardo Andrade for providing the rheological data and aiding in its analysis, and to Carolina Pinta for her help with FTIR analysis. A big thank you to Mariana Matias for her advice on screen printing and to Alexandra, Rafaela, and Francisca for keeping the lab running smoothly and always finding solutions to my challenges.

Finally, a heartfelt thanks to my parents for unwavering supporting my dreams, I carry a part of you with me everywhere I go. To my family, I hope you now have a clearer understanding of what a materials engineer does—if not, you'll just have to see it for yourselves at my defense. A special thanks to my friends, Beatriz Nobre, Rodrigo Barão, Daniela Neves, Manuel Macedo, Leonor Paim, Gonçalo Ramos, Guilherme Valente, Ana Martins, and so many more for making the long hours bearable with laughter and card games.

“To plant a garden is to believe in tomorrow.”

- Audrey Hepburn

"Engineers turn dreams into reality."

- Hayao Miyazaki

ABSTRACT

The growing interest in smart packaging highlights the need to replace critical raw materials in electronic devices with sustainable alternatives, such as cellulose. This study explores CMC/CNF/PPy and CMC/CNF/PANi functional paper as active layers for flexible and environmentally friendly self-standing substrate moisture sensors in smart packaging. Functional inks were formulated, and films were manufactured by doctor blade deposition, followed by screen printing of interdigital electrodes (IDEs). The functional papers were characterized by means of ATR-FTIR, FIB-SEM images, contact angle measurement, tensile tests and I-V curve analysis. The performance of the humidity sensor showed response times between 360-420 s and recovery times up to 1320-1920 s, with sensitivity ranging from 0.597 to 0.6 uA/RH% from 10 to 80 RH%. In addition, the pressure detection tests revealed a sensitivity of 81.7 MΩ/Torr, with response and recovery times of 4.26 and 2.2 seconds, respectively. Despite demonstrating the potential of functionalized paper in smart packaging applications, the low sensitivity of moisture sensors suggests that further optimization of composite composition is needed to improve performance. This work demonstrates that cellulose-based materials can serve as sustainable alternatives in sensor applications, although additional adjustments are needed to improve their sensitivity and reliability in real-world applicability scenarios.

Keywords: Smart Packaging, Resistive Humidity Sensor, Cellulose, Polypyrrole, Polyaniline, Functionalized Paper.

RESUMO

O crescente interesse em *smart packaging* destaca a necessidade de substituir matérias-primas essenciais em dispositivos eletrónicos por alternativas sustentáveis, como a celulose. Este estudo explora papel funcional CMC/CNF/PPy e CMC/CNF/PANi como camadas ativas para sensores de humidade de substrato *self-standing* flexíveis e ecológicos em embalagens inteligentes. Foram formuladas tintas funcionais e os filmes fabricados por deposição por *doctor blade*, seguidos de *screen printing* de elétrodos interdigitais (IDEs). Os papéis funcionais foram caracterizados por meio de ATR-FTIR, imagens FIB-SEM, medição do ângulo de contato, ensaios de tração e análise da curva I-V. O desempenho do sensor de humidade mostrou tempos de resposta entre 240-480 s e tempos de recuperação entre 360-420 s e tempos de recuperação entre 1320-1920 s, com sensitividade de 0.597 a 0.6 uA/RH% de 10 a 80 RH%. Além disso, os testes de deteção de pressão revelaram uma sensibilidade de 81,7 MΩ/Torr, com tempos de resposta e recuperação de 4,26 e 2,2 segundos, respetivamente. Apesar de demonstrar o potencial do papel funcionalizado em aplicações de embalagens inteligentes, a baixa sensibilidade dos sensores de humidade sugere que é necessária uma maior otimização da composição composta para melhorar o desempenho. Este trabalho demonstra que os materiais à base de celulose podem servir como alternativas sustentáveis em aplicações sensor, embora sejam necessários ajustes adicionais para melhorar sua sensitividade e confiabilidade em cenários de aplicabilidade reais.

Palavras chave: Embalagens Inteligentes, Sensor de Humidade Resistivo, Celulose, Polipirrol, Polianilina, Papel Funcionalizado.

CONTENTS

List of Figures

List of Tables

ACRONYMS

AH	Absolute Humidity
CMC	Carboxymethyl cellulose
CNF	Cellulose Nanofibers
IDEs	Interdigitated Electrodes
MFC	Microfibrillated Cellulose
PANi	Polyaniline
PPy	Polypyrrole
RH	Relative Humidity
SP	Smart Packaging
S-S	Self-standing substrate
APS	Ammonium Perdisulfate
HCl	Hydrochloridic acid
CSA	Camphor-sofonic acid
NaCl	Sodium Chloride
ATR-FTIR	Attenuated Total Refectance – Fourier Transform Infrared
SEM	Scanning Electron Microscope

SYMBOLS

Ω	Ohm (unit of resistance)
τ	Shear stress
$\dot{\gamma}$	Shear rate
n	Flow behavior index
k	Consistency coefficient
G'	Storage modulus
G''	Loss Modulus

1 INTRODUCTION

1.1 Smart Packaging

With the evolution of technology and the growing demand for safety and quality of products, improving packaging is an increasingly interesting area of research. Smart packaging is a concept to maintain shelf-life and product quality, provide more valuable information to consumers, enhance safety and better product traceability through the supply chain [1], [2]. For food packaging it contributes to the decrease of food waste and can control food-borne illnesses [3], [4].

Smart packaging encompasses both active and intelligent properties. Preserving and enhancing the quality is related to active properties, such as incorporating active components able to reduce the bacteria in the product [1], [5]. Some examples include moisture regulators, carbon dioxide and scavengers and preservatives [5]. The intelligent part provides information on the product by monitoring its condition and reporting on changes in quality and safety [5], [6], such as time-temperature, gas, pH and freshness indicators, as well as radio frequency identification (RFID) systems [1].

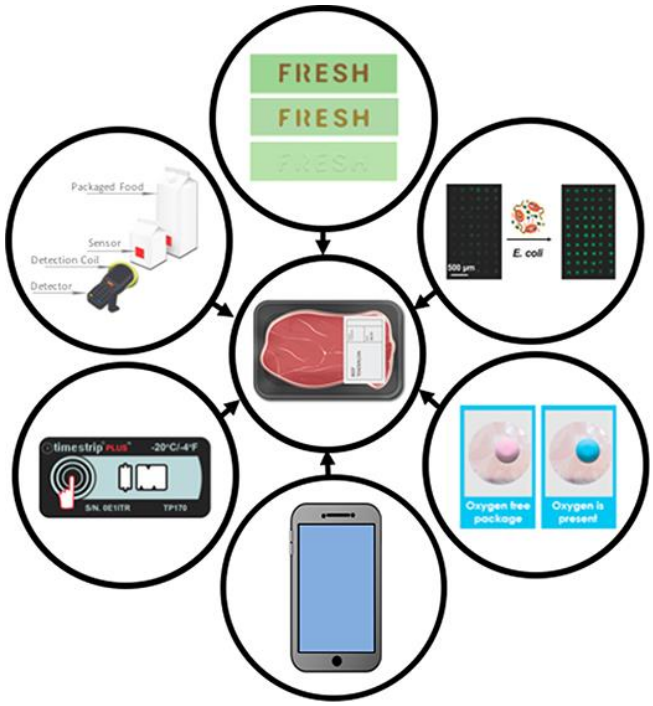

Figure 1 - Schematic on the different sensing features included in a smart packaging device for a meat package [4].

Incorporating smart packaging would significantly improve food chain supply concerns due to real time monitoring capacitating suppliers and consumers of tracking products from

cradle-to-gravel, having complete and valuable information at their disposal and, if possible, access all these through portable devices through the incorporation on the Internet of Things (IoT) [1], [2].

However, it is yet to be achieved a system able to be produced on a large-scale [6]. Also, the raw materials used in similar devices pose a concerning sustainability problem, making the substitution with bio-based and nature-derived materials a focal point, given these would aid in the recyclability, carbon neutrality, food saving and safety [3]. The use of naturally derived materials has increased in interest, with more research and advances [1], even so the cost of current development and manufacturing of these devices poses a challenge in the commercial area [4].

1.2 Humidity Sensors

Humidity sensors are more present in everyday life than people realize since the monitorization of moisture is hugely relevant in various sectors, namely indoor acclimation, medical equipment, and pharmaceutical production and storage [7]. These also apply to the food industry, where storing and transporting certain products in controlled humidity can extend their shelf-life and prevent spoilage [2], [7]. For example, fruits require an elevated humidity level not to lose moisture, which affects their roughness and taste. However, an extreme percentage can increase microbial growth and lead to faster decay [8].

The two methods to measure humidity rely on relative (RH) or absolute (AH) measurements [9], [10]. The first is the most common and represents the moisture in the air compared to the saturated amount in percentage. The former indicates the ratio of the absolute mass of water vapor in the air to the saturated amount at a designated temperature. Relative humidity sensors have a large spectrum of applications due to their simplicity [11] and low cost [7], while absolute humidity sensors are more applicable for the traceability of determined measurements [9].

Several sensor characteristics require special attention to acquire a high-standard functional humidity sensor. The response should be fast, as should the recovery time, while covering a wide range of humidity measures (for example, 10-90%RH), specifically in low humidity. The sensor must be precise, implying a high sensitivity (slope of the output versus input curve) and a small hysteresis (maximum output delta between an up and down cycle of RH%). Repeatability and reproducibility are relevant to the device's reliability, as they measure for short and long-term precision of specific measurements, respectively [7], [9], [11].

Categorization by the transduction mechanism distinguishes humidity sensors into optical, electrochemical, electrical, mass-sensitive, and thermometric [9]. This work focuses on

electrochemical (charge transfers to an electrode as the electroactive transducer material interacts with water vapor) and electrical (water vapor interacts with the surface, generating an electrical change/response) mechanisms [9], [10].

The type of transduction or humidity-sensitive materials utilized classifies the sensor further as composite, an ionic salt, semiconductor, ceramic, metal oxide, carbon-based, and polymer humidity sensors [9]. This research explores polymer-based humidity sensors, which general mechanism relies on the adsorption and desorption of water vapor molecules, resulting in an electrical and physical modification of the sensitive materials properties [10], [12]. According to the electrical response detected, a change in conductivity or dielectric permittivity, the sensor is resistive or capacitive, respectively [12], [13], [14].

1.3 Cellulose and Cellulose-Based Devices

With the rise of necessity for sustainable alternatives to fossil-based polymers, cellulose emerges as a "back to nature" and biomimicking concept, attracting commercial interest [15]–[17]. As the most abundant biopolymer on earth [17]–[19], its biodegradability [15], [20], recyclability [21], biocompatibility [19], [21]–[23] and wide availability transform it into one of the most viable options for sustainable raw materials across several areas [20], as showed in Figure 2. Cellulose has various derivatives, expanding its range of properties and applicability, some examples include nanocellulose, cellulose nanofibers (CNF), microfibrillated cellulose (MFC), carboxymethyl cellulose (CMC), and bacterial cellulose, to list a few [17], [18], [20].

Figure 2 - Sources, properties and main applications of cellulose and its derivatives [20].

Cellulose-based smart packaging applications have increased in number due to its non-toxicity as a natural material [15], [20], [23]. It is an especially attractive material for flexible

sensors, owing to its mechanical properties , lightweight structure, and castability as film [15], [23]. The presence of a lot of hydroxyl groups (-OH) indicates high hydrophilicity, another important quality of cellulose and its derivates, indicating moisture absorption and humidity sensing abilities [18], [23]. The sensing response is highly dependable on the amount of -OH free groups, porosity of the surface and general structure [17]. Nonetheless, the electrical response is not good, as it is a naturally insulating polymer, so it is common for cellulose-base devices to be functionalized with an electrically conductive counterpart [16], [20].

Derivatives as CMC have been engineered to be soluble in water and present a higher reactivity with -COO- (carboxylate group) bond from the carboxymethyl group, facilitating functionalization [20]. However, it displays poor mechanical properties and high hydrophilicity, affecting the lifetime of the device [15]. On the other hand, CNF presents a structural network of fibers, implying enhanced mechanical behavior, even being implemented as reinforcement for composites [16], [22].

1.4 Conjugated Polymers: Polypyrrole and Polyaniline

Conductive polymers emerge in bio-based, electronic and sensor applications as organic substitutes for semiconductors and metals, highlighted by their intrinsic conductivity, simple synthesis, lightweight and environmental stability [24], [25]. The electrical properties derive from the presence of conjugated bonds throughout the backbone structure, in conjugated π polymers, an electrical pathway from free moving delocalized π-electrons on the non-saturated structure creates charge mobility, such as polypyrrole (PPy) and polyaniline (PANi) [22], [24].

Polypyrrole, included in this category, has sparked interest with its easy and adjustable preparation [22] and non-toxicity [26], [27], yet it is not biodegradable [21], it is insoluble [24], [26], thermally instable [21] and brittle [21], revealing its use challenging. On the other hand, polyaniline changes its structure according to oxidation state, leucoemeraldine (fully reduced), emeraldine (partially oxidized) and pernigraniline (completely oxidized) [28]. Emeraldine is the conductive oxidative state, characterized by an emerald color, and presenting benzenoid and quinonoid rings intercalated in its structure [25], [28]. PANi presents similar issues to PPy, in solubility and biodegradability, which chemical modifications and addition of dopants have been explored to enhance [28].

Implementing a composite system with green materials such as cellulose to aid in improving on the lacking properties has been reported. Cellulose and its derivates can improve hydrophilic and mechanical properties, also creating flexible structures [17], [25]. On the other hand, the incorporation of PPy and PANi functionalizes the cellulose, generating an electrically conductive composite from binding insulating and conjugated polymers [20], [22].

1.5 Approach

This work intends to fabricate a humidity sensor based on nature derived functional materials with application in smart packaging, considering the importance of humidity for the preservation and quality maintenance of goods, by monitoring shelf-life of products, increasing the safety of its consumption and decreasing food waste.

Cellulose and its derivatives act as a base material to build a sustainable device, avoiding the use of critical raw materials. To enhance its electrical properties, cellulose is polymerized *ex-situ* with conjugated polymers PPy or PANi, creating a functional composite, the active layer of the sensor. To create this film, the first step entails formulating a functional water-based ink containing cellulose nanofibers (CNF), carboxymethylcellulose (CMC) and one of the conducting polymers. The conjugated polymers present some toxicity, therefore a small amount, less than 1% of the functionalized ink, is incorporated. Doctor blade technique is implemented to cast the self-standing substrates in a glass substrate, then once fully dried, IDEs are printed as contact with the active material. As the humidity increases, the cellulose matrix will swell, imposing a larger distance between the charge carriers of the conducting polymers, increasing the resistance.

This document details the methods and materials implemented in this work in Section 2, following an in-depth analysis and discussion of the results obtained on Section 3, and finishing the final remarks and future perspectives for this project. In the Appendix is present supportive information regarding all the sections.

2 METHODOLOGY

2.1 Device Fabrication

The device has an active layer as a self-standing substrate of cellulose and conductive polymers and interdigitated electrodes, (Fabrication Process Schematic). The process for creating the paper-based device is described in the A. Paper-based Devices Fabrication.

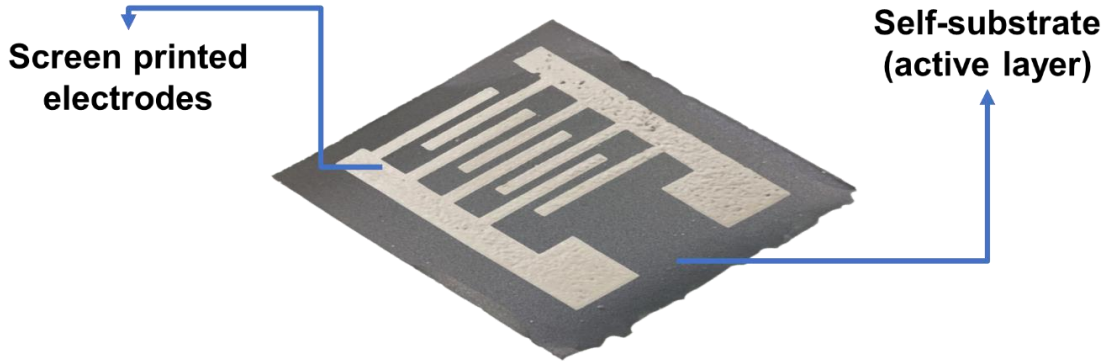

Figure 3 - Schematic of a self-standing substrate-based device, identifying the different layers.

2.1.1 Polypyrrole and Polyaniline Powder Synthesis

Synthesizing these polymers involves three steps: preparing the oxidant and monomer solution, setting up the reaction system by mixing the solutions, and cleaning and drying the powder. For polypyrrole, the oxidant solution contains 0.548 M APS and 0.429 mM HCl 37%, and the monomer solution contains 1.44×10^{-3} mM pyrrole, considering deionized water as the solvent. Next, the solutions are transferred to an ice bath at 0 to 4°C. After cooling down, the oxidant solution is poured into the monomer solution, which synthesizes for 30 minutes. Then, the powder is extracted through filtration and cleaned with deionized water and absolute ethanol. The product is dried in an oven at 60°C for at least 24 hours. For polyaniline, the oxidant solution contains 0.4 M APS, and the monomer solution contains 0.1 M CSA and 0.4 mM Aniline, with a base of deionized water and absolute ethanol in a 1:1 ratio. The synthesis occurs for 1 hour and 30 minutes or when the solution presents an emerald-green color. Methanol replaces absolute ethanol in the cleaning process, and drying conditions are maintained.

2.1.2 Functional Ink Formulation

The inks are prepared in a 250 mL beaker, starting with deionized water, then adding the cellulose components, carboxymethyl cellulose (CMC), then cellulose nanofibers (CNF) or

cellulose microfiber (MFC), and lastly the conductive polymer powder, polypyrrole (PPy) and polyaniline (PANi). Reagents incorporate the ink while mechanically stirred by a LED overhead stirrer 40 L, RSLAB-13/40L with a crossed stirrer, 5x40 cm, SS attachment, at 350 rpm. After fully incorporating the reagents, the ink stirs for an additional 4 hours and is stored on a fridge at 5ºC.

2.1.3 Functional Self-standing substrate Fabrication

A double-sided tape (1065 µm in height and approximately 1.25 cm in width) is placed around the substrate on a 10 cm by 10 cm glass to define the height and area for ink deposition. Inks, previously fabricated, were used to produce the self-standing substrates with a K101 Control Coater System, using meter bar 8 to deposit a 100 µm wet film at a speed of 2 mm/s. The substrate is placed on the coating area with another 10 cm by 10 cm glass as support. The rod is attached and placed on the top of the substrate. Around 10 mL of ink is deposited on the edge of the tape. Once the applicator coats the entire area, reposition the rod to the top of the tape again and transfer the excess ink dragged from the edge of the substrate to the beginning of the coating area. This process repeats, resulting in various layers of ink. The substrate dries in an open space but with the protective grid on top. Once the substrate is dry (one to two days), carefully remove it with the help of a scalpel and store it in a desiccator.

2.1.4 Electrode Deposition

Each self-standing substrate is cut into 2 cm x 2 cm samples. Electrodes deposition occurs by screen printing with a 120T mesh, with one to two layers of ink on each sample. Silver and carbon ink are the two commercial inks used, along with two distinct design patterns, interdigital and coaxial, with in-between distances of 3, 6, and 10 mm. For the coaxial design, a paintbrush applies the ink onto a tape masked sample.

2.2 Materials and Characterization

A detailed list of reagents used in this work is in section Materials.

To characterize the inks, self-standing substrates and devices, tests in rheology, composition (ATR-FTIR Spectroscopy), morphology (SEM), hydrophilicity/hydrophobicity and wettability (contact angle, stability tests), mechanical (tensile tests), electrical (I-V curves), and humidity and pressure sensing were conducted. Further details on these tests and equipment are in C. Characterization.

3 | Results and Discussion

Excluding the polymer synthesis, the first step to the fabrication process is the ink formulation. Multiple formulations were developed, considering the resulting self-standing substrates. CMC is the primary source of cellulose for almost all the formulations (Figure 4), but the second source started to be MFC yet, due to the high roughness of the resulting self-standing substrates, it was switched with CNF. One of the primary measures to enhance the ink was the introduction of mechanical stirring with the overhead stirrer during the addition of the reagents, improving uniformity and being less time-consuming. To avoid clusters in the self-standing substrates, sifting of the polymer powder was introduced; however, it was a tiring process and was replaced with additional stirring for 4 hours after the complete addition of the reagents.

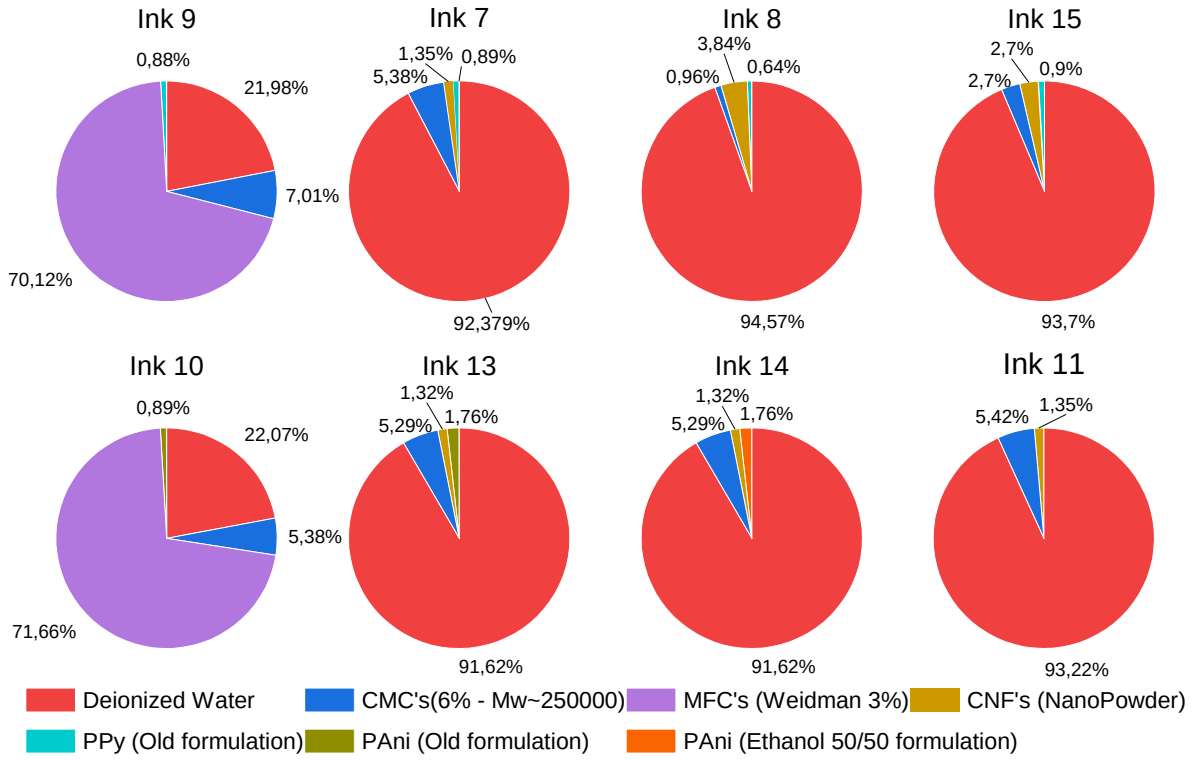

Figure 4 - Functional-Ink formulations of the most relevant inks for this work. Polypyrrole inks in the first row and polyaniline on the second.

Regarding the functional component of the inks, the polymerization process was *ex-situ* due to the simplicity of the powder synthesis and scale-up process allowing to produce substantial amounts of polymer. *In-situ* polymerization was attempted at the end of the lab work (reported in In-situ *polymerization* of inks) considering it is the most common process in

similar studies and should present a more uniform distribution of polymer through the

Sample ID	Ink	Rod (µm)	Speed (mm/s)	Layers	Wet Weight (g)	Dry Weight (g)	Thickness (mm)	Resistivity (1cm) - Porous (MΩ)	Resistivity (1cm) - Glossy (MΩ)	Resistivity Cross Section (MΩ)
S_I11_1065+100um_2sp_4l	11	100	2	4	5.5084	0.409	0.058	-	-	-
S_I11_1065+50um_2sp_4l	11	50	2	4	5.8096	0.4321	0.076	-	-	-
S_i13_1065+100um_2sp_4l	13	100	2	4	6.108	0.5859	0.306	8-55	14-68	5-60
S_i13_1065+50um_2sp_4l	13	50	2	4	5.3926	0.5327	0.179	8-15	10-53	10-70
S_i14_1065+100um_2sp_4l	14	100	2	4	-	0.4369	0.168	22-53	22-115	88-128
S_i14_2130+100um_2sp_4l	14	100	2	4	11.6342	1.0938	0.256	50-130	21-80	11-60
S_i15_1065+100um_2sp_4l	15	100	2	4	4.3741	0.3309	0.057	84-115	90-130	18-90
S_i15_1065+50um_2sp_4l	15	50	2	4	4.2978	0.3244	0.064	91-120	88-115	18-88
S_I7_1065+100um_2sp_2l	7	100	2	2	-	0.3886	0.206	61-195	83-120	29-115
S_I7_1065+50um_2sp_2l	7	50	2	2	-	0.5322	0.237	67-200	90-200	33-80
S_i7_2130+100um_2sp_4l	7	100	2	4	12.7342	1.1786	0.156	69-135	31-100	10-40
S_I8_1065+100um_2sp_4l	8	100	2	4	5.8147	0.3692	0.085	64-120	40-110	17-80
S_I8_1065+50um_2sp_4l	8	50	2	4	5.065	0.3878	0.063	59-120	67-100	19-70

Figure 5 - Table with a base characterization of different self-standing substrates.

composite, improving conductivity. However, mechanical stirring resulted in higher binding of the polymer structures during polymerization, resulting in a gel instead of an ink. Another issue with this process was the impossibility of removing unreacted reagents from the ink. An alternative was to remove it directly from the substrate through dipping in methanol; yet, due to the hydrophilicity of the self-standing substrates (discussed further in 3.3 Hydrophilicity and wettability) this process would be destructive.

3.1 Rheological Study of Functional Ink

The optimization of functional substrates is a critical aspect in the development of advanced materials and devices. One of the key steps in achieving this goal is to understand and control the properties of the functional ink used in substrate fabrication. The rheological behavior of these inks plays a crucial role in determining their printability, stability, and overall performance during the manufacturing process. From Figure 6 A, shear-thinning behavior is present in all inks, since shear rate increases, and viscosity decreases. Inks 8 and 9 have high viscosity, meaning that spreading requires more tension and the ink keeps its structure at rest, providing higher control of the printing process. On the other hand, inks 7, 14 and 15 have low viscosity, flowing easily which reduces control over spreading in doctor blade. The graph area outlined corresponds to ideal behavior for doctor blades [29], which all inks intercept, excluding ink 14. Ink 7 and 15 do present a more fluid behavior than ideal, while ink 8 and 9 have a better fit. Since a low spreading speed of 2 mm/s is used and the substrate had a delimited area for ink deposition, more fluidity did not have such a negative effect in terms of spreading control, so ink 7 was a good fit, since after doctor blade it would spread and fill the deposition area. Ink 9 was indeed the best for printing, but MFCs affect the surface roughness, making the resulting substrate unsuited for screen printing of electrodes. This was the main reason for switching to CNFs, and it was never possible to match one of the new formulations with this one.

Non-Newtonian behavior is further confirmed by shear stress vs. shear stress graph (Figure 6 B). The need for lower pressure/stress to flow inks 8 and 9 and the opposite for inks 7, 14 and 15 is also exhibited. This data was fitted with the mathematical model of Herschel-Bulkley ($\tau(\dot{\gamma}) = \tau_y + k\dot{\gamma}^n$) [30] and the results are presented on Table 1. Inks 8 and 9 shows a shear stress limit, as τ_0 is superior to 1 Pa, indicating a yield stress material behavior. Regarding the viscoelastic nature of the inks, ink 7 and 14 have a superior loss modulus (G'') to the storage modulus (G'), characteristic of viscoelastic liquids. The remaining inks first have a higher G', and then transition to a superior G'', changing from a viscoelastic gel to a liquid behavior. In this case the structure starts to break at the shear stress where G' and G'' are equal, which is at

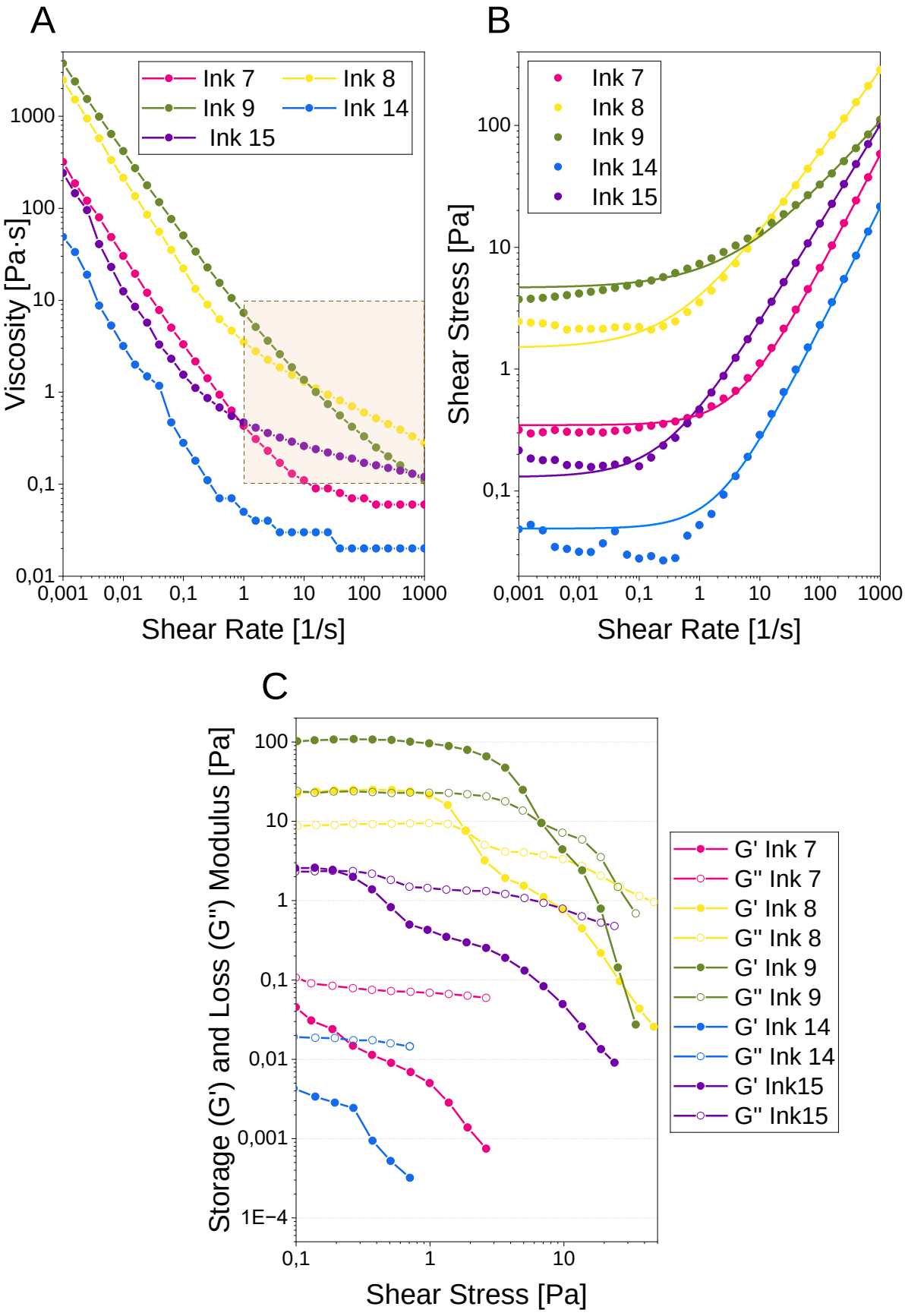

Figure 6 - Flow curve (A), shear stress vs. shear rate (B) and storage and loss modulus vs. shear stress (C) graphs of inks 7, 8, 9, 14 and 15.

0.18814 Pa, 1.8891 Pa and 6,7938 Pa for ink 15, 8 and 9 respectively. As viscoelastic gel is more suited for doctor blade printing, inks 8, 9 and 15 fit this model (Figure 6 C).

Table 1 - Herschel-Bulkley mathematical model fitting parameters for inks 7, 8, 9, 14 and 15.

Ink	τ_0	k	n	R^2
7	0,3472±0,01316	0,07764±9,21792E-4	0,95677±0,00177	0,99998
8	1,49333±0,1745	2,54321±0,0484	0,68298±0,0028	0,99989
9	4,6448±0,24141	2,07455±0,11174	0,56664±0,00819	0,99872
14	0,04916±0,0114	0,02239±6,56846E-4	0,9931±0,00438	0,99988
15	0,13008±0,01063	0,36482±0,00156	0,81442±6,43817E-4	1

3.2 Morphology and Composition of Self-standing substrates

To ensure the bonds between the different components and the general structure of them, ATR-FTIR spectroscopy of different self-standing substrates was conducted. Due to the similarities between CMC and CNF structures (Figure 9), and the general overlapping and merging of peaks, analysis is complex.

On a first look at the spectrum (**Error! Reference source not found.**), a broad peak in the 3600-3000 cm^{-1} ranges, an area associated with hydrogen bonds [31]. This peak refers to O–H stretching of the hydroxyl groups present in both CMC and CNF and represents absorbed water in the composite which is highly likely from the high amount of water in the ink formulation, and absorption from the environment [32]–[35]. A slight shoulder on the right side of the peak indicates the presence of N–H stretching from the conjugated polymers in each substrate [35]. At around 2870 cm^{-1}, the C–H stretching peak is present, a bond present in all the components [33], [34], [36], [37]. Unexpectedly, a peak at 2360 cm^{-1} is registered, associated with the physisorption of CO_2, presumably due to trapped air during the drying process of the self-standing substrate [38].

In the fingerprint range highlighted in Figure 7, a weak peak at 1725 cm^{-1} in the spectra from self-standing substrate from ink 14, is attributed to C=O stretching from carboxymethyl group in CMC [35]. A strong sharp peak in 1580-1587 cm^{-1} represents C=C and C–N stretching of aromatic ring bonds in both PPy and PANi [34], [39]. At 1411-1413 cm^{-1} is a medium peak present in all the self-standing substrates, which represents C–H_2 bending from the cellulose components [35]. This peak can also be assigned to C–N^+ stretching from PANi for self-standing substrate from ink 14 [40]. A shoulder on the left of the peak is attributed to C–H bending

vibrations [35]. Next, the peak at 1314-1320 cm^{-1} corresponds to C–H and C–O aromatic ring vibrations from CNF [36]. A right shoulder on the previous peak in self-standing substrate from ink 14 spectra is representative of C–N stretching in secondary amine group on aromatic rings in PANi [41]. However, this shoulder is also weakly present on self-standing substrates with PPy in which is assigned as C–N and C–H in-plane deformation [37].

The last strong peak at 1020-1027 cm^{-1} is ascribed to C–H deformation vibration from PPy (for S-S from Ink 7, 8 and 15), [39] C–C and C–OH stretching from cellulose [34], [36]. There are two left shoulders, at 1095-1104 cm^{-1} and 1152-1158 cm^{-1} respectively assigned to C–O stretching [35] and C–O–C asymmetric stretching vibrations of β glycosidic linkage from the cellulose components [34] and, C–OH stretching vibrations [33]. A medium sharp peak at 892-897 cm^{-1} represents of C–H out-of-plane deformation or C–C in-plane bending of pyrrole ring [37], and C–H out of plane bending of aromatic rings (PANi) [41]. C–H stretching and C–H out-of-plane ring deformation is the assignment for peak 779-783 cm^{-1} [37], [39].

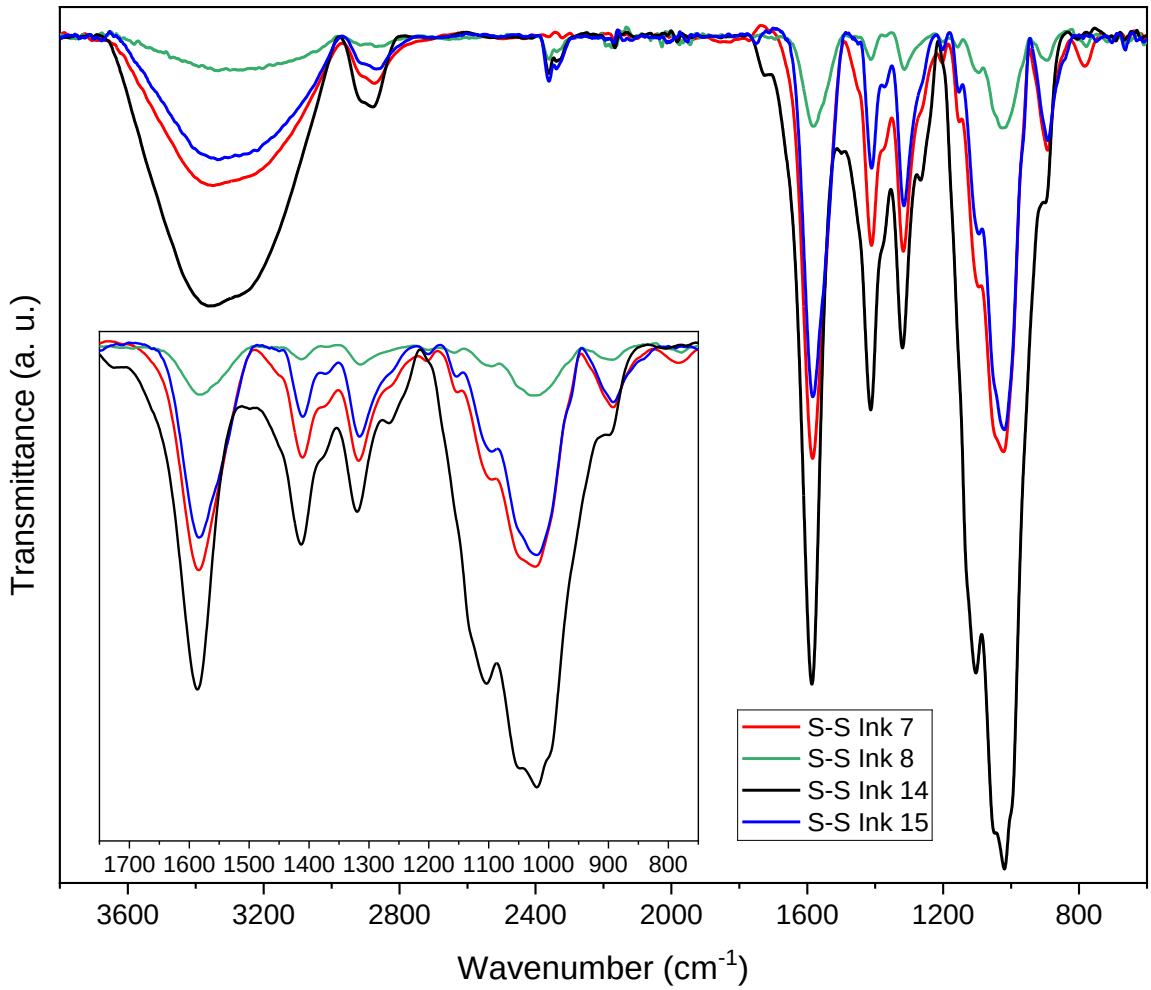

Figure 7 - ATR-FTIR spectra of self-standing substrates 7 (red), 8 (green), 14 (black) and 15 (blue) and specifically the fingertip section (1750-750 cm^{-1}) on insert figure.

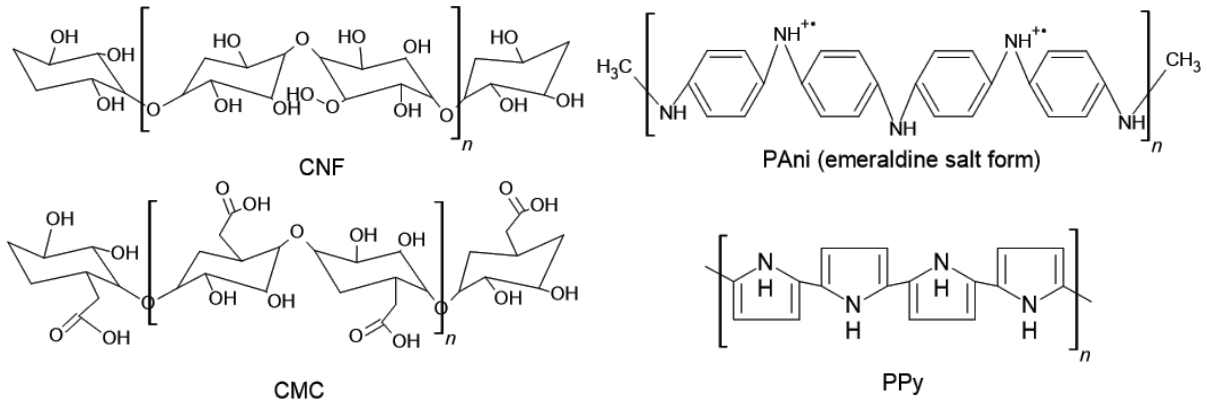

Figure 8 - Structure of the self-standing substrates' components.

Accounting for this analysis, all the components are detected in the spectrum with cellulose being more present as expected due to corresponding to at least 90% of the composite material. Hydrogen bonding is the main structural bond of the self-standing substrate, being represented in the broad peak at 3335 cm^{-1}. The peaks and respective assignments, as well as a detailed graph of each samples' spectrum, are summarized in a table in ATR-FTIR Analysis.

To analyze the morphological structure of the self-standing substrate FIB-SEM microscope images were taken. Liquid nitrogen was used to break the samples to visualize the cross section of the self-standing substrates. Fos self-standing substrates from ink 7 and 8 a conductive gold layer was deposited to improve the quality of high magnification images. The results are displayed on Figure 9, presenting the cross section and surface structures of self-standing substrates from inks 7, 8, 15 and 14. In general, a smooth base structure of CMF and CMC is visible, with polymer agglomerates on the surface and in between layers. In Figure 9 B, CNFs are observed peaking in the cross section and it is the only samples where it was visible even though ink 7 has the least amount of CNF. This could be a small agglomerate that was not properly mixed in the ink, since the remaining samples all show uniformity of the cellulose base. However, areas in bright white, almost as if glowing, are associated with the presence of nanofibrils, and these are visible across all samples [42].

It is noticeable the difference in porosity and thickness, particularly in comparison with self-standing substrate from ink 14. The films with PANi displayed a higher roughness, due to the lower dispersiveness of the PANi powder compared to PPy, resulting in higher thickness and presence of agglomerates, which is clear in Figure 9 G. The porous surface of the films is visible on Figure 9 A, C and E, exhibiting a heterogeneous topography, and an overall roughness, despite on a macro level appearing very smooth. This uneven distribution of the conducting polymer can cause an heterogenous electrical response. However, this roughness can be positive for humidity sensing [43], as a higher surface area [10] can better absorb water molecules.

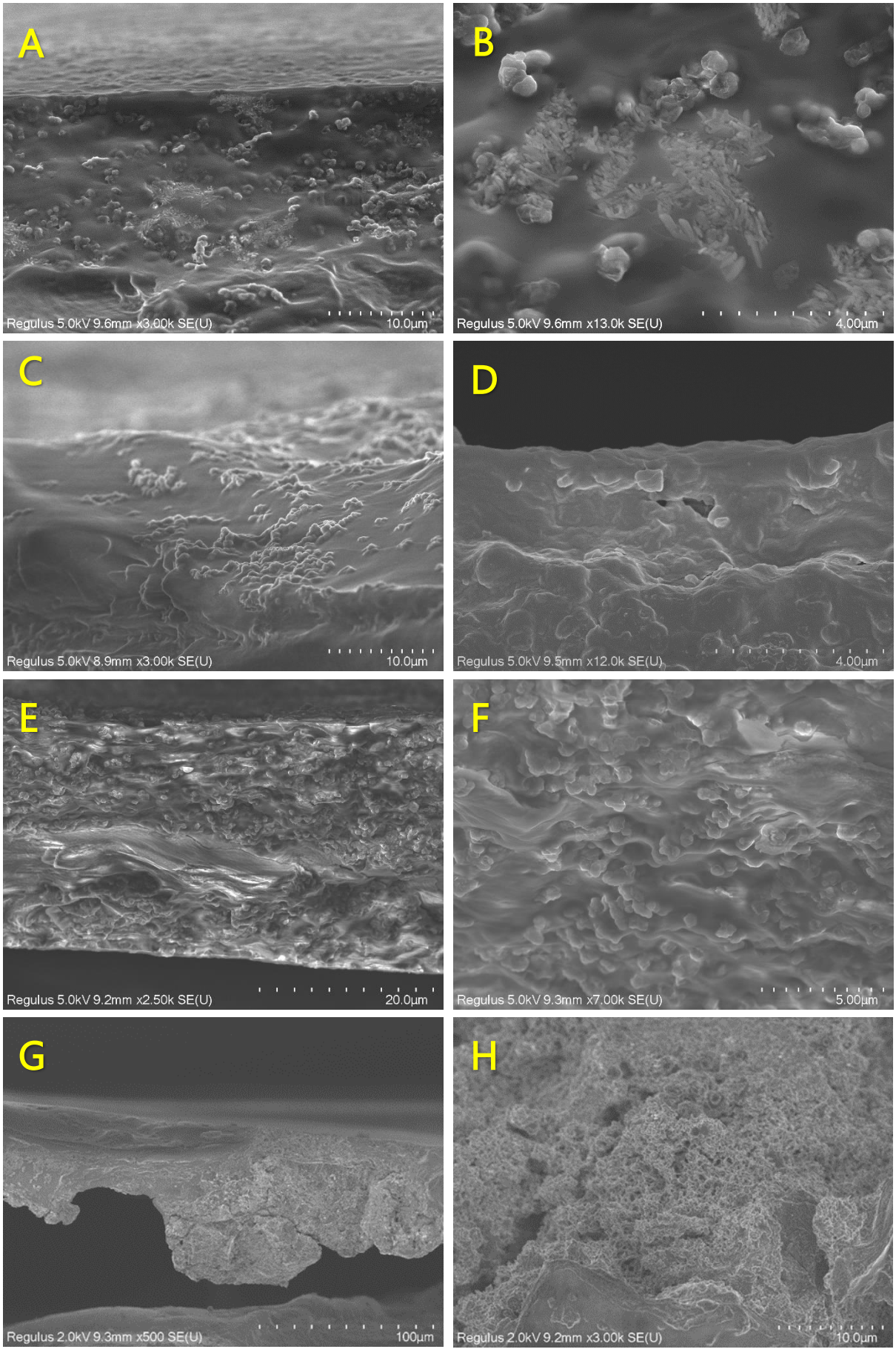

Figure 9 - FIB-SEM images of cross section from self-standing substrates 7 (A, B), 8 (C, D), 15 (E, F) and 14 (G, H).

The structures of PANi are visible (Figure 9 H), and the polymer is not forming long fiber structures, contrary to expected. [44] This information aligns with issues experienced during polymer synthesis, whose time had increased far more than the established time, from around 1 hour and 30 minutes to over 5 hours. For the remaining films, PPy presents a granular spherical structure, as expected [45], clearly visible on the surface of the three different samples (Figure 9 B, D and F).

3.3 Hydrophilicity and wettability

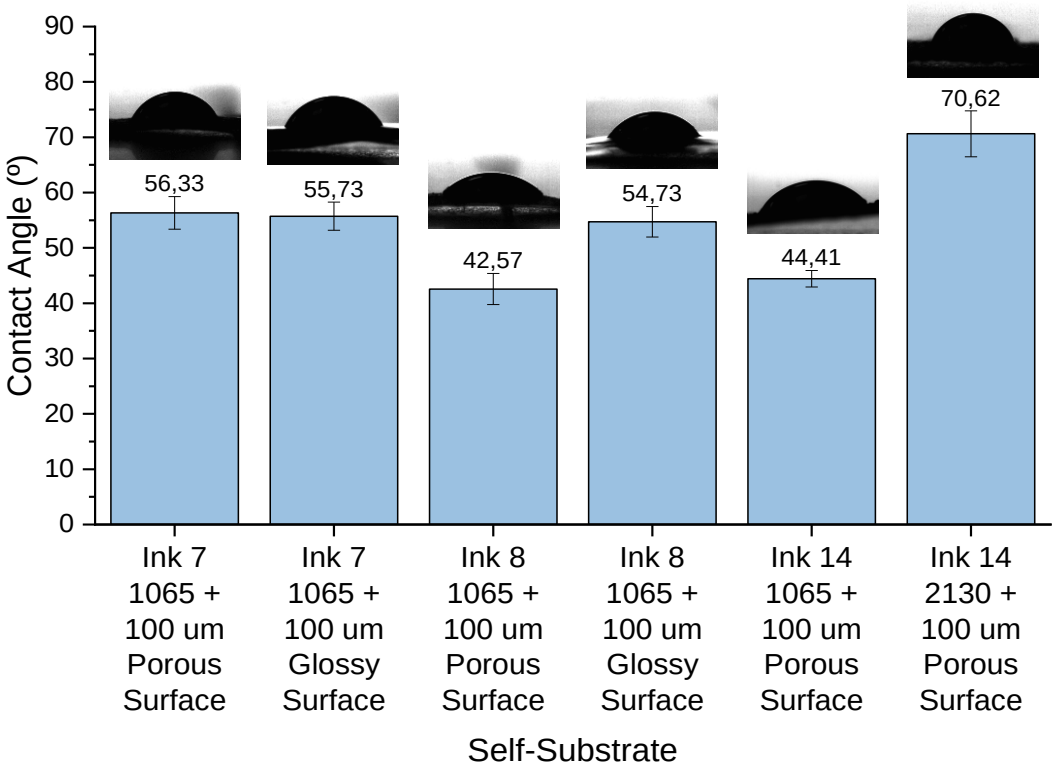

Figure 10 - Contact angle values for self-standing substrates from ink 7, 8 and 14 with different thickness and surfaces. The X axis labels refer to the ink of the substrate, the height of the tape (1065 and 2130), the doctor blade height and surface of the film.

To attest the hydrophilic properties of the self-standing substrates, water contact angle measurements were conducted. Porous and glossy surfaces were tested for self-standing substrates from ink 7 and 8, while for ink 14 only the porous since in this self-standing substrate the two surfaces are very similar, and the high porosity made the measurements difficult to obtain requiring more replicates being more time consuming.

In Figure 10 the values for each self-standing substrate and respective surface are represented. All values are below 90º, indicating hydrophilic behavior and high wettability, which is expected, due to the high amount of cellulose in the composition, and desirable for humidity

sensing [46]. Comparing the two surfaces of self-standing substrates from ink 7 and 8, it was presumed the glossy surface presents a higher contact angle on account of lower roughness, a situation that is true for self-standing substrate 8. However, for ink 7 film, the opposite is seen, the porous surface contact angle is superior. Despite this difference the values exhibit proximity to each other and to the contact angle for ink 8´s glossy surface. PPy would increase the contact angle, as PPy films present high hydrophilic values from 65 to 80º [47]. CMC and CNF have low values of contact angle and are reported to lower the value in composite films. Kim et al. presents a CMC film with 33.9º [48] while CNF presents slightly lower values at 33º [36] , which is consistent to our results, as CNF content is superior in ink 8.

Concerning the self-standing substrate from ink 14, for the same thickness as previous films, it is similar, particularly to ink 8. This is unexpected given surface morphology differences, even so higher overall percentage of cellulose compared with the other substrates can lower this measurement. The highest contact angle registered is in the thicker films from ink 14, presenting the most roughness of all the before mentioned. For emeraldine salt PANi films, a contact angle of 65 to 86º [49] and 73.7 ± 13.13º [50] was obtained in other studies, so the influence of higher amount of PANi on the surface could justify this result. After comparing all samples, the surface morphology likely contributes to some discrepancies in the correlations, as it introduces errors.

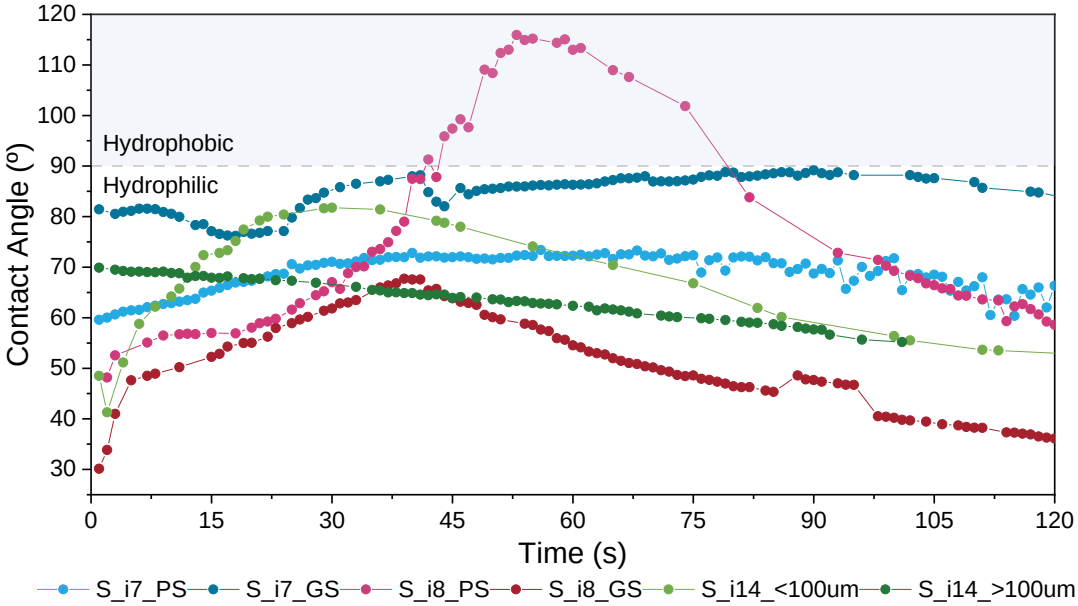

Figure 11 - Dynamic contact angle for self-standing substrates from ink 7 (blue), 8 (pink) and 14. (green).

In Figure 111 the water contact angles throughout two minutes are plotted. Movement of the self-standing substrate defining the baseline for the measurement made it difficult, and manual adjustments were necessary, requiring for a lot of sections of data had to be removed. Hydrophilic behavior is further proved by this data, despite the initial rise associated with an

advancing contact angle, all the samples, excluding the porous surface of ink 7 films, always present values below 90º.

The reaction in the presence of water was further studied through stability tests, dropping set amounts of water on the self-standing substrates. In Fig. 12 A the samples have only been in contact with deionized water for 5 minutes, yet there is substantial and higher damage done as the amount increases. Not one sample completely maintained its structural integrity, with ink 7 and 15 films showcasing large holes, as well as ink 14 in a smaller scale. Self-standing substrates from ink 8 kept the smoothest appearance, despite a small hole in the 2.5 mL samples.

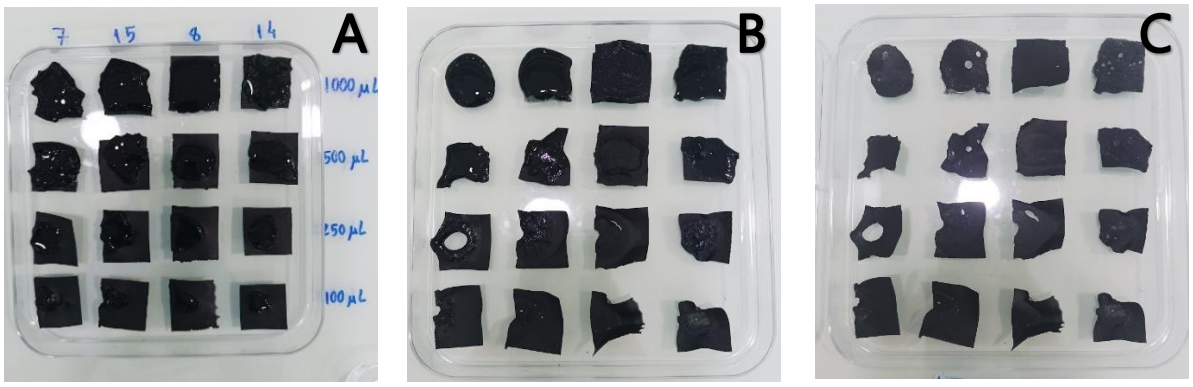

Figure 12 - Pictures at 5 minutes (A), 5 hours (B) and 47 hours (C) after deposition of water on self-standing substrates samples from inks 7, 15, 8 and 14.

3.4 Mechanical Behavior of self-standing substrates

Tensile test to self-standing substrate and papers are depicted in Figure 13. At first impression, the failure for all samples is catastrophic indicating fragile behavior, except for high thickness self-standing substrate from ink 7 that did not experience failure, due to the sample slipping from the holding grips, and Whatman paper grade 1, which exhibits some tolerance and ductility.

The values of tensile stress, strain and Young's modulus (Figure 14) give more insight on the mechanical properties of the samples. The difference in CMC:CNF ratio between self-standing substrates from ink 7 and 8 is evident, with the latter exhibiting 18% increase in Young's modulus, 1% in maximum strain and 67% in maximum tensile stress. CNFs present superior mechanical properties to CMC [48], [51], validating this result. Film thickness plays a relevant role in the mechanical properties, with an increase in Young's modulus by 48% and 45% for ink 7 and 14 substrates, respectively. Due to the issues regarding the fracture of higher thickness films from ink 7, it is not possible to compare the other parameters. However, for ink 14 maximum tensile stress is not affected, while maximum strain increases by 3%.

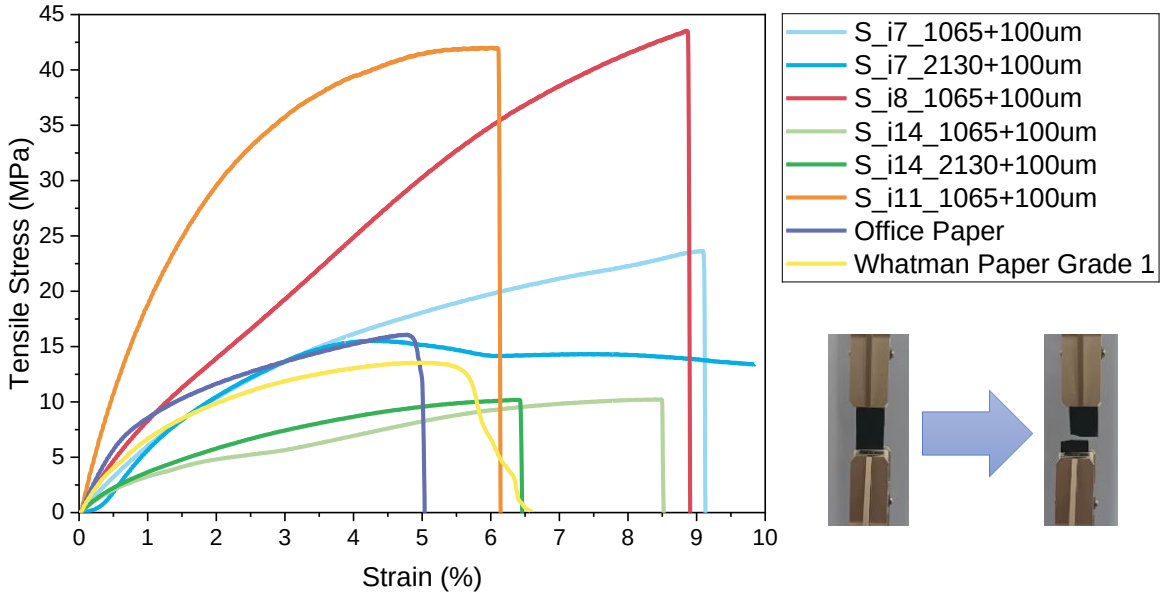

Figure 13 - Tensile test curves for self-standing substrates from ink 7 (blue), 8 (red), 14 (green) and (11 (orange), and office paper and Whatman paper grade 1. On the corner, a representative example of the visual fracture of the self-standing substrates. The legend corresponds to "Substrate_Ink_TapeHeight+RodHeightum".

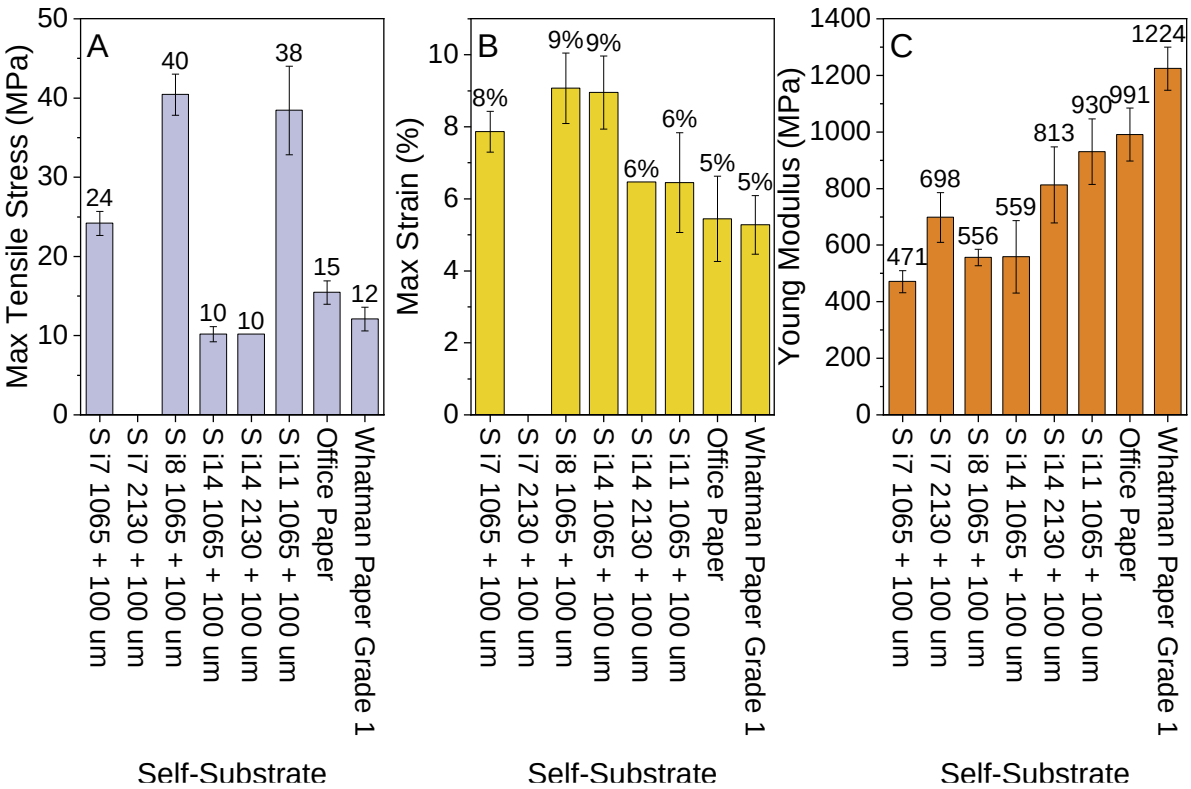

Figure 14 - Max tensile stress (A), max strain (B) and Young's modulus (C) for self-standing substrates, office paper and Whatman paper grade 1.

Ink 11 has the same formulation as inks 7 and 14, without the addition of polymers, and is used as a comparative tool to evaluate the effect of polymers on mechanical properties.

PPy decreased maximum tensile stress by 58%, and Young's modulus by 97%, while slightly increasing strain by 2% [22], [52]. PANi presents similar changes with 280%, 66% and 3% differences, respectively. Ink 14 has double the amount of polymer compared to ink 7, so it is not a proportional comparison and a possible explanation for such a low maximum tensile stress. Comparing generic paper with self-standing substrate samples, max strain and tensile stress (excluding films from ink 14) are lower, and Young's modulus is higher.

3.5 Electrical Response

To assess the electrical properties of the functional self-standing substrates, I-V curves were measured from -2 V to 2 V and the resistance calculated in a sample the size of the device (2 x 2 cm) connecting with flat copper clips. A representative result for all types of self-standing substrates ink 7, 8, 14 and 15 is showed in

Figure 15 - I-V curve of self-standing substrates (black) and resistance (blue).

which demonstrate a high variability of resistance, that was also present in multimeter measurements, and a lack of sensitivity and precision, as the curve spikes repeatedly. This will reflect in sensing behavior, in linearity and sensitivity. The low amount of polymer present in self-standing substrates justifies the high resistance obtained. This electrical response can be justified with the heterogeneous distribution of PPy and PANi on the surface and cross section, as seen in Figure 9. CMC and CNF have an isolating nature decreasing further the conductivity. Due to the low dimension of the thickness of the film it is possible for all this data to be noise due to poor contact with the clamps.

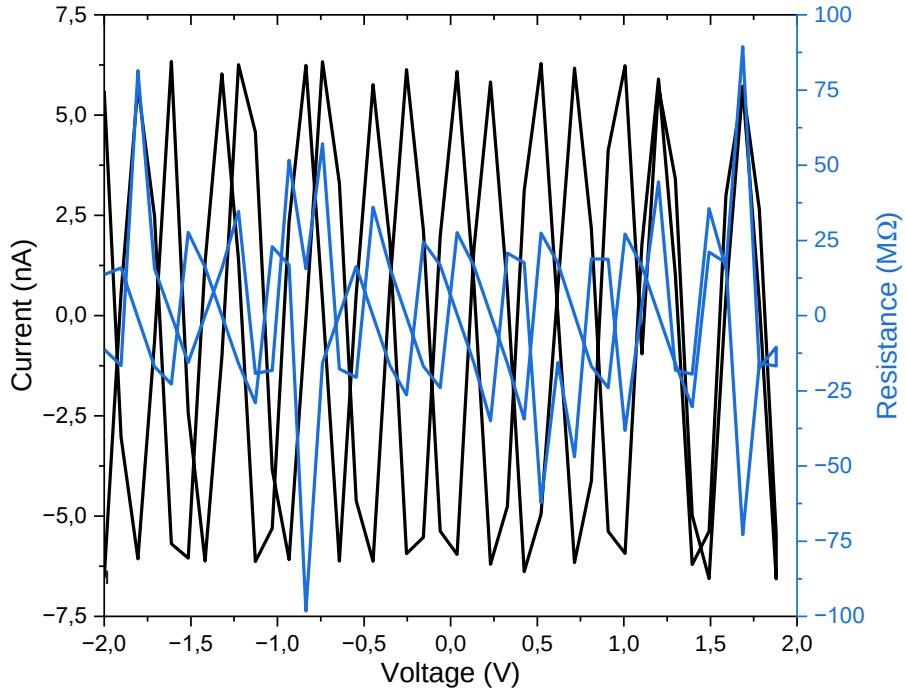

Figure 15 - I-V curve of self-standing substrates (black) and resistance (blue).

3.6 Sensing Performance

The device's simplicity, as the entire functionalized paper acts as the sensor, does not require complex printing, embedding of external sensors, or additional manufacturing steps for incorporation into packaging materials, and reduces material and production costs. It eliminates the need for separate sensors, wiring, or complex electronics, making it a cost-effective solution for mass-produced smart packaging.

3.6.1 Humidity Sensor

All devices tested used the same IDEs design and silver ink, and self-standing substrates from ink 7, 8, 14 and 18, that respectively correspond to devices 59, 33, 104 and 105. Ink 18 was only developed after the first results were analyzed and it is the same formulation as ink 7, but with 3wt% of NaCl to help with saturation of the sensor. Due to the time needed for each test it was not possible to do different thickness films or a self-standing substrate from ink 11, which could help us understand the effect of these factors in humidity sensing.

The testing range went from 10 to 80 RH%, with a focus on low humidity as this is the objective of current research on humidity sensing. The humidity varied from 10 to 60 RH%, yet due to the need for long periods of time for the chamber to achieve 10 RH% not all the tests were able to achieve this value. Also, during the two months of use of the chamber, less

accurate results were registered over time, which affected the results. In Figure 16, the sensing response is visible for a low humidity cycle from 10 to 60 RH%. The I-V curves of the self-standing substrates are highly resistive and present high variability as reported in the previous section.

Device 59 was the first to be tested, and despite the variability, a clear trend is visible from 180 to 360 minutes matching the humidity variation. The sensitivity increases from 40 to 60 RH% compared to 10 to 40 RH%, as the output difference also increases. However, after the resistance value rises again and slightly increases, indication possible oversaturation, making the sensor unable to release the water it has absorbed. This behavior is more typical of cellulose, which is good for absorption and has trouble in desorption, like the sensor response. This sensor presents extremely high resistance measurements due to the use of 10 MΩ resistance in the voltage divider, which does not represent the real resistance of 20 to 100 MΩ. This makes a direct comparison with other devices is incorrect as the resistance was switched with a 10kΩ.

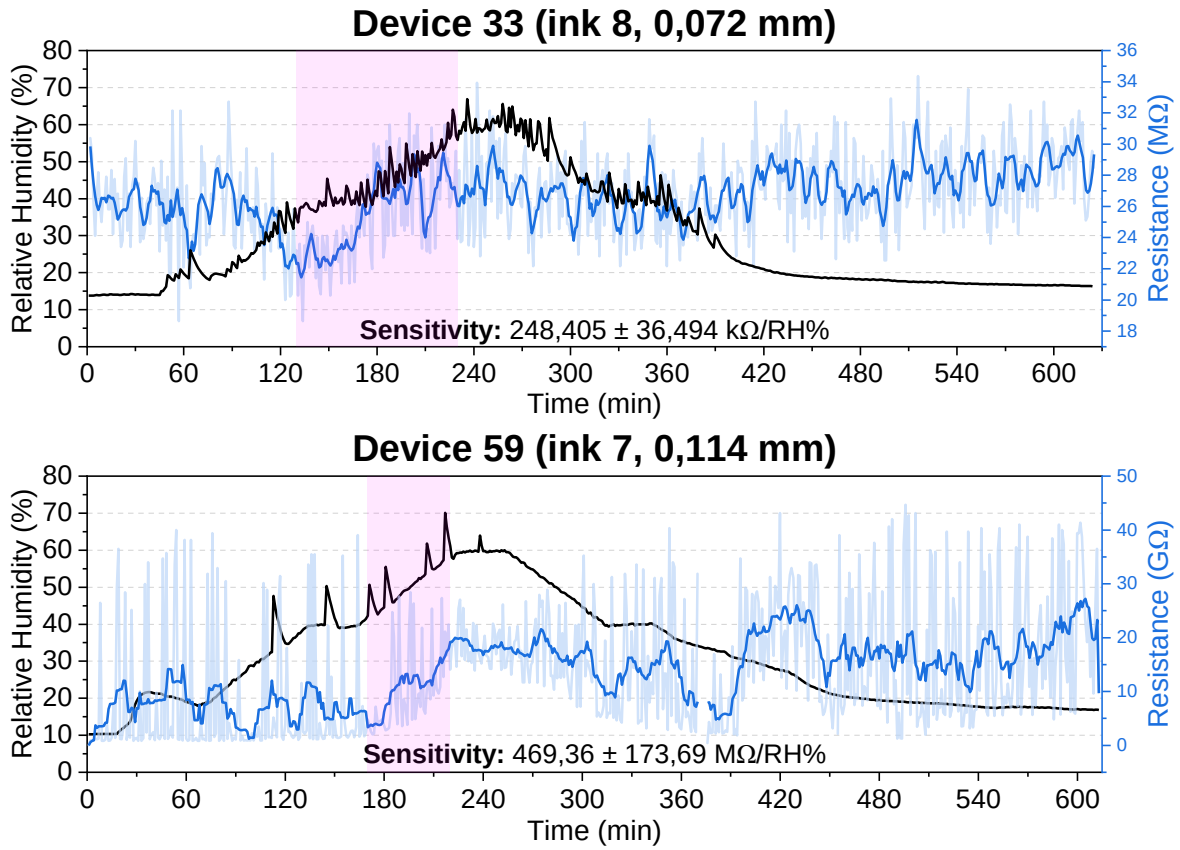

Figure 16 - Humidity sensing results of devices 33, 59 in a 10 to 60 RH% cycle. In light blue is the real measurement of resistance while in dark blue is a smoothed curve to help understand the tendency of the data. The area in pink is the data used to measure the sensitivity of the sensor.

Device 33 was the next subject and showed similar issues, as saturation after the highest humidity point remained and the only from 35 to 45 RH% was there a correlating response in

resistance, as after this it stagnates and increases slightly. The less precise relative humidity registered also contributes to this result, as higher humidity is being reached sooner than planned, resulting in earlier oversaturation.

Data and analysis on devices 104 and 105 are on Appendix G. Humidity Sensing.

To test the widest range possible, a test with a ramp from 10 to 80 RH% was performed, registering the recovery time as well as response time. To obtain these measurements after the humidity stabilizes at 80%RH the chamber stops decreasing the RH quickly and measuring the electrical response over time to obtain the recovery time values, visible in Figure 17 highlighted by the green area. As a significant change in humidity occurs and a current response matches it the time between the two events is the response time.

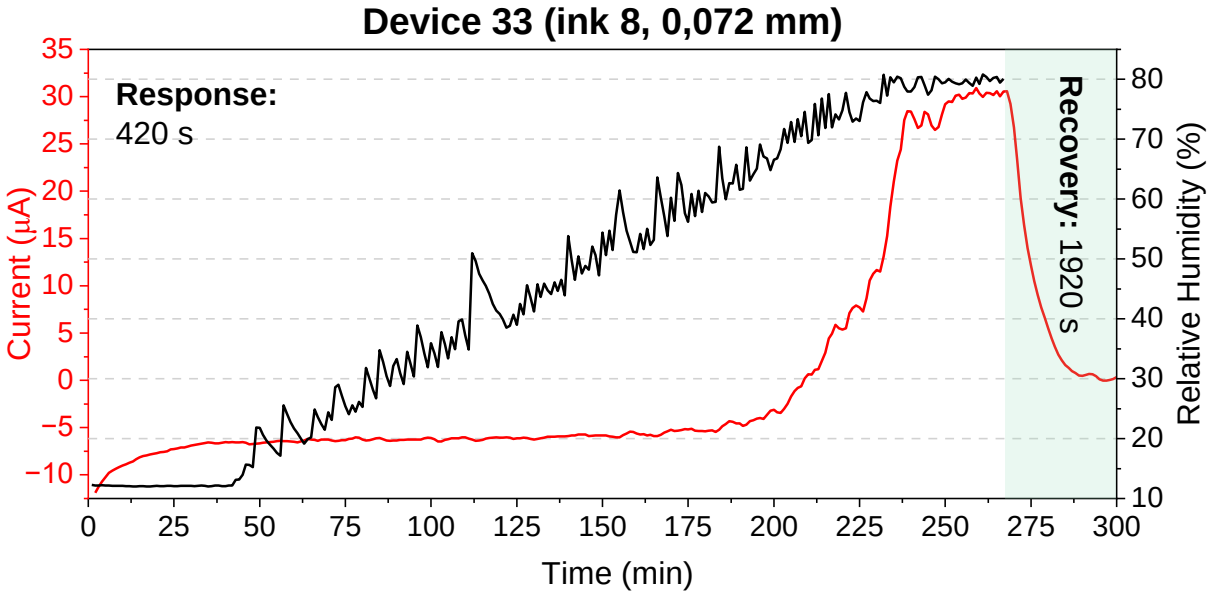

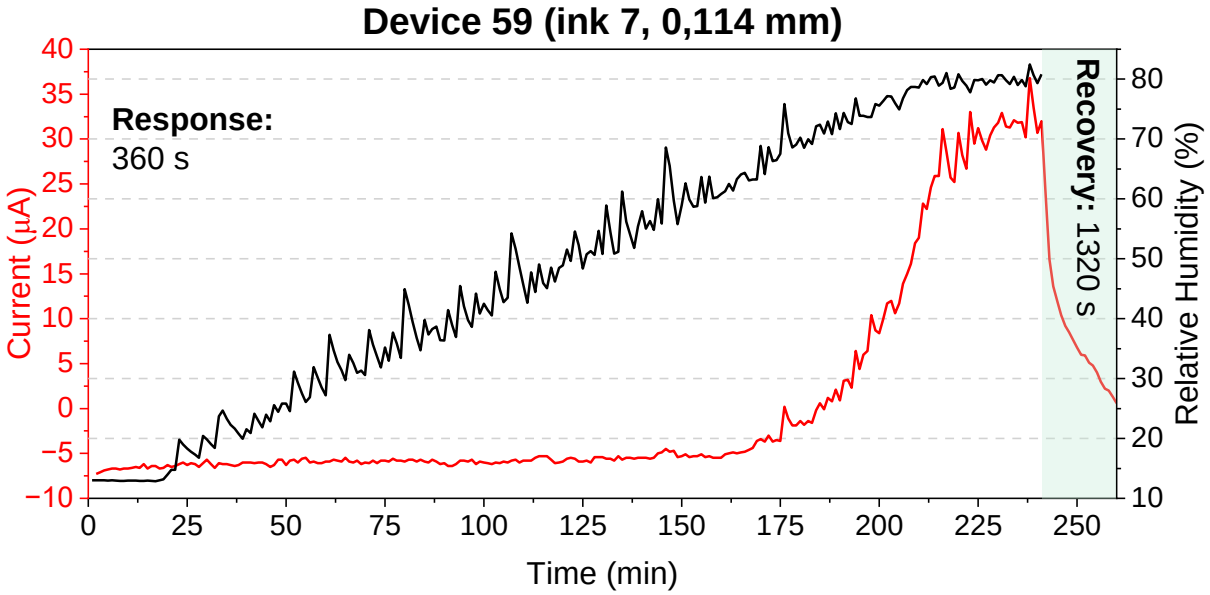

Figure 17 - Devices 33 and 59 sensing response to a 10 to 80 RH% ramp with recovery and response time.

Device 59 presents a quicker response time than device 33 with 6 and 7 minutes, respectively, which is longer than ideal, yet some sensors with cellulose and conductive polymers present similar values, as seen in Table 2. The recovery time is higher than desired as well, 22 and 32 minutes, for device 59 and 33, respectively. As these parameters were only measured for this test, it would be important to repeat it with replicas of the devices to get a more accurate value. Regarding sensitivity, the values are very similar with 0.6 and 0.597 μA/RH% for devices 59 and 33 which is particularly to the PPy modified filter paper device show in Table 2. In

Figure 18, selected values from the previous graph (Table 3) are plotted from where the sensitivity was measured and the R^2 values close to 1 show very good linearity.

Table 2 - Humidity sensors with similar components to devices discussed.

Sensor Type	Substrate Material	Electrode Material	Sensitivity	Humidity Range	Response / Recovery Time	Reference
Resistive	PANI–CMC	Silver	~20000 Ω/RH	25-75%	10 s (at 75% RH) / 90 s (at 75% RH)	[53]
Voltage	PPy modified filter paper	Copper	0.61 V/RH%	33-98% RH	43 s / 51 s	[46]
Capacitive	MCM-41/PPy	Carbon	~119 pF/RH%	11–95% RH	~915 s / ~100 s	[54]
Resistive	Cellulose/PA	-	70.9 kΩ/RH %	2-50% RH	Short cycling: 90s / 87s Long cycling: 370s / 1490s	[55]
Capacitive	Nanoscale PPy *in-situ* polymerized cellulose	Gold	11.74 pF/RH%	64-80% RH	~418 s / ~418 s	[56]

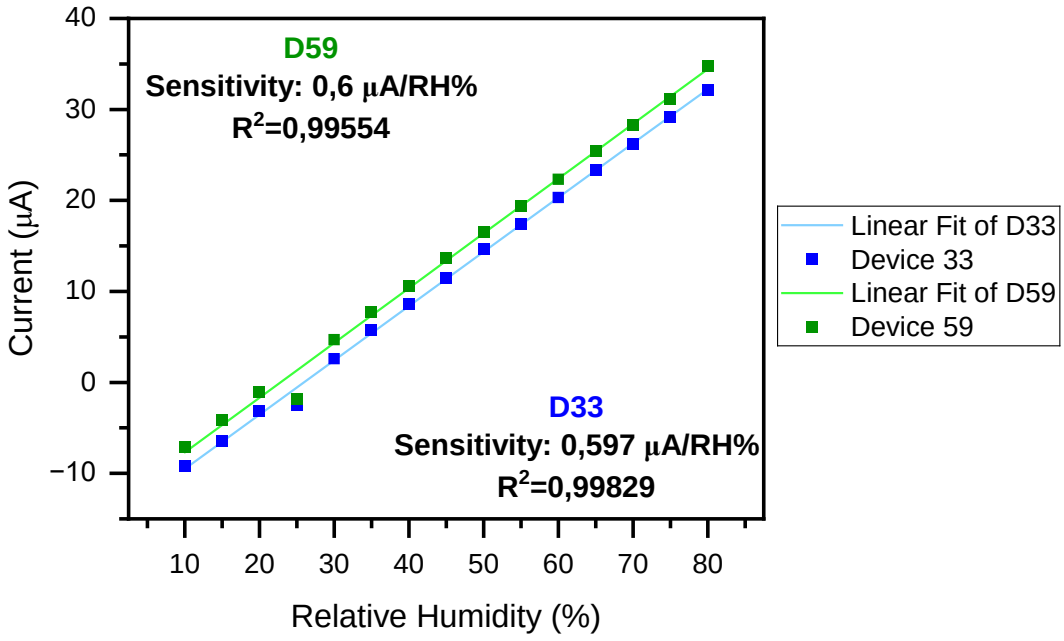

Figure 18 - Sensitivity and linearity of device 33 and 59 in 10 to 80 RH% ramp.

Table 3 - Current values for devices 33 and 59 from 10 to 80 RH%.

RELATIVE HUMIDITY (%)	CURRENT (µA)	
	Device 59	Device 33
10	-7,1	-9,2
15	-4,2	-6,5
20	-1,1	-3,2
25	-1,8	-2,5
30	4,7	2,6
35	7,7	5,7
40	10,6	8,6
45	13,6	11,5
50	16,5	14,6
55	19,4	17,4
60	22,3	20,3
65	25,4	23,3
70	28,3	26,2
75	31,1	29,1
80	34,8	32,1

Figure 19 - Pictures of sensors before and after being exposed to 80RH%.

After being exposed to such high humidity device 59 and 104 wrinkled like paper, device 33 presents slight oxidation on the electrodes, and device 105 tore due to its fragile state as it absorbed more water, as seen in Figure 19. Wrinkling is not problematic as the self-standing substrates are very flexible, allowing them to be 'molded back' into shape when stored. It has a preferential direction to curl inwards due to the CNF positions in the structure due to the doctor blade deposition movement. The silver ink was expected to possibly oxidize, which is why carbon ink devices were fabricated, as carbon is more inert to interact with water molecules, yet there was no time to test these devices.

To correlate these results with the composition of the self-standing substrate of each device is difficult, as RH cycles varied in accuracy from test to test, and there are circuit differences for some devices. Devices 59 and 33 have quicker recovery, which can be an effect of PPy, as device 104 has the longest recovery (Figure 24). Despite this, it has the shortest response time, that could be due to its porous morphology. Since it is not known how NaCl is integrating the composite, it is not clear if increasing its amount could help the sensing response as the present data shows otherwise. As previously mentioned, integrating different salts could also be a path for improvement.

3.6.2 Pressure Sensor

The pressure sensing mechanism of these devices derives from the charge transfer as the molecules are pressured, closing the distance between the PPy and PANi molecules, inducing a change in resistance as seen in Figure 20. For pressure sensing only a few tests were done with device 33 (ink 8, 0.072 mm, 4 cm^2) with the system shown in Pressure Sensing Testing Set-Up. The response to different weights was tested, yet with only 100g a result was obtained (Figure 20). Considering the devices surface area and the gravity acceleration, the sensitivity is

81.7 MΩ/Torr. The response and recover time are quick, only at 4.26 and 2.2 seconds, respectively. There is a higher hysteresis visually compared with finger pressure results, meaning the output after recovery is different to the start of response output.

The devices responded well to finger pressure in the interdigital area of the electrode, specifically ungloved. The pressure input on the device was not measured, therefore it is not possible to calculate the sensitivity for these results. However, it is possible to characterize the response and recovery time, as well as visually assess the hysteresis. These results are dependent of the circuit, reason why the resistance in used is indicated in the title of each graph. With a 100kΩ resistance, the output difference is small, indicating higher sensitivity. There is small hysteresis in all the results, only the first graph appears to have a negative value which is not possible, so the first cycle did not fully recover. Response and recovery time are similar, varying from 5 to 7 seconds and 1 to 3 seconds, respectively. Since these measurements were not timed and done arbitrarily it is normal for differences in cycles.

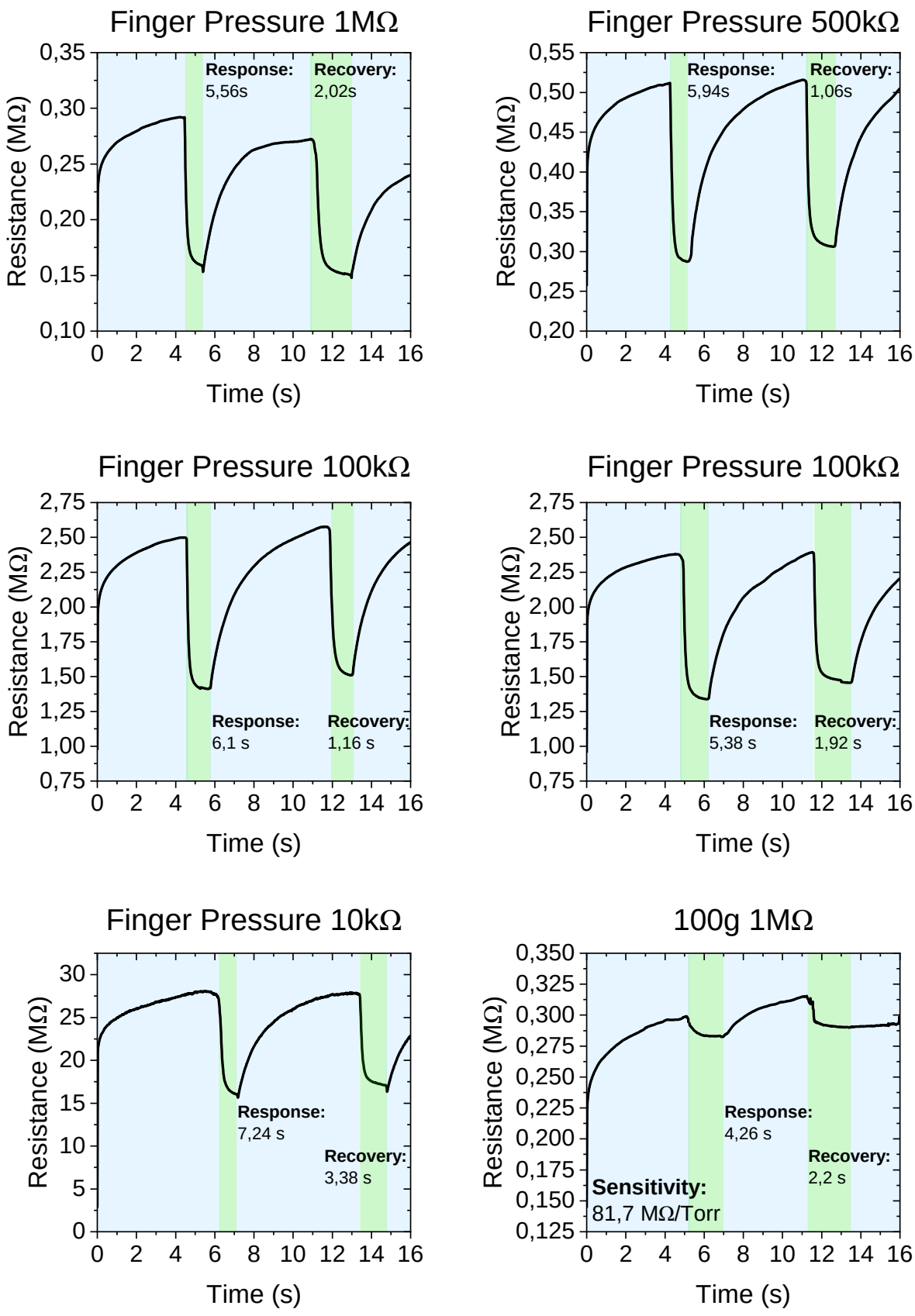

Figure 20 - Pressure sensing results for device 33 with finger pressure and 100g weight.

4 | Conclusions and Future Prospects

This work is intended to develop a humidity sensor for smart packaging composed of natural, sustainable and recyclable functional materials. Cellulose was integrated as the base material for the functional paper, namely CMC, CNF and MFC, which were functionalized through the incorporation of conjugated polymers PANi and PPy by *ex-situ*. The fabrication of the active substrate included formulating the functional ink, casting by doctor blade, obtaining the self-standing substrate and screen printing of IDEs with commercial silver and carbon ink. This process is simple, easily reproducible and up scalable, generating interest for industrial applications.

Rheological studies of functionalized inks indicate the suitability for doctor blade technique for all the main inks, excluding ink 14 due to the dispersiveness of PANi. The characterization of the fabricated self-standing substrates reveals the functionalization was successful as ATR-FTIR spectroscopy indicates the presence of hydrogen bonding, and through FIB-SEM images show the binding of the functionalization of the cellulose and the distribution of conducting polymer throughout the cross section. Contact angle measurements convey the hydrophilic behavior of films, an important characteristic for humidity sensing, specifically in the porous surface where IDEs are placed. However, stability tests express the fragility of the films in direct contact with water, which is revealed to be problematic for high humidity sensing.

Tensile tests of films reveal catastrophic failure and a higher tensile strength and strain than regular office paper. A larger amount of CNF in the composition implies a stronger self-standing substrate compared to CMC, while the incorporation of polymers decreases the tensile strength and Young's modulus but slightly increases max strain. I-V curves reveal a lack of precision and low conductivity from self-standing substrates, indicating possivle low sensitivity of the devices.

Few humidity sensing tests were performed, and various issues raised with the equipment and set-up which were not resolved at the end of this work. These preliminary results (Table 4) confirm the device has humidity sensing properties and response time is not very far from some sensors with similar compositions (Table 2). Sensitivity is also good compared to similar sensors, as well as linearity in the 10 to 80 RH% range (

Figure 18). However, recovery time needs to be improved, as oversaturation makes the sensors recover slowly and the response inaccurate in decreasing RH. Structure integrity at high humidity should also be a concern for devices including PAni and salt, as well as increased sensitivity in low humidity specifically.

Table 4 - Humidity sensing results for sensitivity, response and recover time.

Device	Sensitivity	Response Time (S)	Recovery Time (S)
33	248,405±36,494 kΩ/RH% (40 to 60RH%) 0.6 μA/RH% (10 to 80 RH%)	420	1920
59	[469,36±173.69]x10^3 kΩ/RH% (40 to 60RH%) 0.597 μA/RH% (10 to 80 RH%)	360	1320
104	-18,2±19,75 kΩ/RH% (40 to 60 RH%)	240	>3840
105	39,85±18,38 kΩ/RH% (40 to 60 RH%)	480	2460

Pressure sensing results with a 100g weight reveal sensitivity of 81,7 MΩ/Torr, response and recovery time of 4,26 and 2,2 seconds, respectively. Finger pressure presented good results, yet it was not possible to calculate the sensitivity due to not measuring the amount of pressure applied.

Possible ways to improve this work are as follows:

- **Addition of salts:** Device 105 had only 2,7%wt of sodium chloride, an increase could aid in oversaturation. Attempting other non-toxic salts like magnesium sulphate.
- **Increase in polymer loading:** current inks have a very small amount of PPy and PANi, and its increasing will improve conductivity.
- ***In-situ* polymerization:** Most of the reported works with cellulose and polymers implement *in-situ* polymerization, as the polymer more easily can incorporate the cellulose structure, with stronger bonds and uniformly distributed. The protocol used had several issues and it was not possible to attempt other possibilities.
- **IDEs material inert to water:** Opting for carbon ink or even laser-induced-graphene (LIG) would decrease the possibilities of oxidation at high humidity. Considering smart packaging applications, silver ink should be replaced due to its toxicity.

Considering even further in the future, testing for other sensing responses such as temperature and pH can improve its versatility, acquiring multi-purpose status. Currently the application focuses on the intelligent component of smart packaging, a system including an active

mechanism as microbial growth, and an easy interpretation system as color codes would decrease the distance for an industrial and commercial implementation.

BIBLIOGRAPHY

[1] D. Schaefer and W. M. Cheung, "Smart Packaging: Opportunities and Challenges," *Procedia CIRP*, vol. 72, pp. 1022–1027, 2018, doi: 10.1016/j.procir.2018.03.240.

[2] S. Chen, S. Brahma, J. Mackay, C. Cao, and B. Aliakbarian, "The role of smart packaging system in food supply chain," *J. Food Sci.*, vol. 85, no. 3, pp. 517–525, 2020, doi: 10.1111/1750-3841.15046.

[3] N. Halonen *et al.*, "Bio-Based Smart Materials for Food Packaging and Sensors – A Review," *Front. Mater.*, vol. 7, no. April, pp. 1–14, 2020, doi: 10.3389/fmats.2020.00082.

[4] H. Yousefi, H. M. Su, S. M. Imani, K. Alkhaldi, C. D. Filipe, and T. F. Didar, "Intelligent Food Packaging: A Review of Smart Sensing Technologies for Monitoring Food Quality," *ACS Sensors*, vol. 4, no. 4, pp. 808–821, 2019, doi: 10.1021/acssensors.9b00440.

[5] U. Amin *et al.*, "Biodegradable active, intelligent, and smart packaging materials for food applications," *Food Packag. Shelf Life*, vol. 33, no. January, 2022, doi: 10.1016/j.fpsl.2022.100903.

[6] M. A. Sani, M. Azizi-Lalabadi, M. Tavassoli, K. Mohammadi, and D. J. McClements, "Recent Advances in the Development of Smart and Active Biodegradable Packaging Materials," *Nanomaterials*, vol. 11, no. 5, pp. 1–34, 2021, doi: 10.3390/nano11051331.

[7] T. Delipinar, A. Shafique, M. S. Gohar, and M. K. Yapici, "Fabrication and Materials Integration of Flexible Humidity Sensors for Emerging Applications," *ACS Omega*, vol. 6, no. 13, pp. 8744–8753, 2021, doi: 10.1021/acsomega.0c06106.

[8] A. U. Alam, P. Rathi, H. Beshai, G. K. Sarabha, and M. Jamal Deen, "Fruit quality monitoring with smart packaging," *Sensors*, vol. 21, no. 4, pp. 1–30, 2021, doi: 10.3390/s21041509.

[9] G. Korotcenkov, *Handbook of Humidity Measurement*. 2019.

[10] H. Farahani, R. Wagiran, and M. N. Hamidon, *Humidity sensors principle, mechanism, and fabrication technologies: A comprehensive review*, vol. 14, no. 5. 2014.

[11] X. Aeby, J. Bourely, A. Poulin, G. Siqueira, G. Nyström, and D. Briand, "Printed Humidity Sensors from Renewable and Biodegradable Materials," *Adv. Mater. Technol.*, vol. 8, no. 5, 2023, doi: 10.1002/admt.202201302.

[12] Z. Chen and C. Lu, "Humidity sensors: A review of materials and mechanisms," *Sens. Lett.*, vol. 3, no. 4, pp. 274–295, 2005, doi: 10.1166/sl.2005.045.

[13] L. Huang, Q. Hu, S. Gao, W. Liu, and X. Wei, "Recent progress and applications of cellulose and its derivatives-based humidity sensors: A review," *Carbohydr. Polym.*, vol. 318, no.

April, p. 121139, 2023, doi: 10.1016/j.carbpol.2023.121139.
[14] M. Sajid, Z. J. Khattak, K. Rahman, G. Hassan, and K. H. Choi, "Progress and future of relative humidity sensors: a review from materials perspective," *Bull. Mater. Sci.*, vol. 45, no. 4, 2022, doi: 10.1007/s12034-022-02799-x.
[15] Y. Zhao *et al.*, "Eco-friendly and intelligent cellulosic fibers-based packaging system for real-time visual detection of food freshness," *Chem. Eng. J.*, vol. 474, no. September, p. 146013, 2023, doi: 10.1016/j.cej.2023.146013.
[16] K. Heise *et al.*, "Nanocellulose: Recent Fundamental Advances and Emerging Biological and Biomimicking Applications," *Adv. Mater.*, vol. 33, no. 3, 2021, doi: 10.1002/adma.202004349.
[17] Z. Li *et al.*, "Green and sustainable cellulose-derived humidity sensors: A review," *Carbohydr. Polym.*, vol. 270, no. June, p. 118385, 2021, doi: 10.1016/j.carbpol.2021.118385.
[18] H. Pirayesh, B. D. Park, H. Khanjanzadeh, H. J. Park, and Y. J. Cho, *Cellulosic material-based colorimetric films and hydrogels as food freshness indicators*, vol. 30, no. 5. Springer Netherlands, 2023.
[19] J. Fu, Z. Pang, J. Yang, F. Huang, Y. Cai, and Q. Wei, "Fabrication of polyaniline/carboxymethyl cellulose/cellulose nanofibrous mats and their biosensing application," *Appl. Surf. Sci.*, vol. 349, pp. 35–42, 2015, doi: 10.1016/j.apsusc.2015.04.215.
[20] R. Yekta, R. Abedi-Firoozjah, S. Azimi Salim, A. Khezerlou, and K. Abdolmaleki, "Application of cellulose and cellulose derivatives in smart/intelligent bio-based food packaging," *Cellulose*, vol. 30, no. 16, pp. 9925–9953, 2023, doi: 10.1007/s10570-023-05520-1.
[21] A. M. Salem, A. R. Mohamed, and A. Y. Yassin, "The effect of low concentrations of polypyrrole on the structural, thermal, and dielectric characteristics of CMC/PPy blends," *J. Mater. Sci. Mater. Electron.*, vol. 34, no. 20, pp. 1–13, 2023, doi: 10.1007/s10854-023-10938-1.
[22] M. Lay, J. A. Méndez, M. Delgado-Aguilar, K. N. Bun, and F. Vilaseca, "Strong and electrically conductive nanopaper from cellulose nanofibers and polypyrrole," *Carbohydr. Polym.*, vol. 152, pp. 361–369, 2016, doi: 10.1016/j.carbpol.2016.06.102.
[23] X. Guan *et al.*, "Flexible humidity sensor based on modified cellulose paper," *Sensors Actuators, B Chem.*, vol. 339, no. March, 2021, doi: 10.1016/j.snb.2021.129879.
[24] T. Nezakati, A. Seifalian, A. Tan, and A. M. Seifalian, "Conductive Polymers: Opportunities and Challenges in Biomedical Applications," *Chem. Rev.*, vol. 118, no. 14, pp. 6766–6843, 2018, doi: 10.1021/acs.chemrev.6b00275.
[25] Y. A. Anisimov, R. W. Evitts, D. E. Cree, and L. D. Wilson, "Polyaniline/biopolymer composite systems for humidity sensor applications: A review," *Polymers (Basel).*, vol. 13, no. 16, 2021, doi: 10.3390/polym13162722.
[26] L. Hao, C. Dong, L. Zhang, K. Zhu, and D. Yu, "Polypyrrole Nanomaterials: Structure, Preparation and Application," *Polymers (Basel).*, vol. 14, no. 23, 2022, doi: 10.3390/polym14235139.
[27] A. L. Pang, A. Arsad, and M. Ahmadipour, "Synthesis and factor affecting on the conductivity of polypyrrole: a short review," *Polym. Adv. Technol.*, vol. 32, no. 4, pp. 1428–1454, 2021, doi: 10.1002/pat.5201.
[28] M. Beygisangchin, S. A. Rashid, S. Shafie, and A. R. Sadrolhosseini, "Polyaniline Thin Films

— A Review," *Polymers (Basel).*, vol. 13, pp. 1–46, 2021.
[29] A. Glasser, É. Cloutet, G. Hadziioannou, and H. Kellay, "Tuning the Rheology of Conducting Polymer Inks for Various Deposition Processes," *Chem. Mater.*, vol. 31, no. 17, pp. 6936–6944, 2019, doi: 10.1021/acs.chemmater.9b01387.
[30] L. R. d. C. Moraes, H. Ribeiro, R. J. E. Andrade, and M. F. Naccache, "Rheology of amino-functionalized graphene oxide suspensions in hydrogels," *Phys. Fluids*, vol. 36, no. 1, 2024, doi: 10.1063/5.0185524.
[31] D. Murphy and M. N. de Pinho, "An ATR-FTIR study of water in cellulose acetate membranes prepared by phase inversion," *J. Memb. Sci.*, vol. 106, no. 3, pp. 245–257, 1995, doi: 10.1016/0376-7388(95)00089-U.
[32] M. Consumi, G. Leone, G. Tamasi, and A. Magnani, "Water content quantification by FTIR in carboxymethyl cellulose food additive," *Food Addit. Contam. - Part A Chem. Anal. Control. Expo. Risk Assess.*, vol. 38, no. 10, pp. 1629–1635, 2021, doi: 10.1080/19440049.2021.1948619.
[33] N. Habibi, "Preparation of biocompatible magnetite-carboxymethyl cellulose nanocomposite: Characterization of nanocomposite by FTIR, XRD, FESEM and TEM," *Spectrochim. Acta - Part A Mol. Biomol. Spectrosc.*, vol. 131, pp. 55–58, 2014, doi: 10.1016/j.saa.2014.04.039.
[34] X. Guo, L. Liu, J. Wu, J. Fan, and Y. Wu, "Qualitatively and quantitatively characterizing water adsorption of a cellulose nanofiber film using micro-FTIR spectroscopy," *RSC Adv.*, vol. 8, no. 8, pp. 4214–4220, 2018, doi: 10.1039/c7ra09894d.
[35] W. Lewis, "Ultraviolet Spectroscopy," *Paint Testing Manual*. pp. 545–546, 2009, doi: 10.1520/stp37187s.
[36] M. Jonoobi, J. Harun, A. P. Mathew, M. Z. B. Hussein, and K. Oksman, "Preparation of cellulose nanofibers with hydrophobic surface characteristics," *Cellulose*, vol. 17, no. 2, pp. 299–307, 2010, doi: 10.1007/s10570-009-9387-9.
[37] A. Kausaite-Minkstimiene, V. Mazeiko, A. Ramanaviciene, and A. Ramanavicius, "Evaluation of chemical synthesis of polypyrrole particles," *Colloids Surfaces A Physicochem. Eng. Asp.*, vol. 483, pp. 224–231, 2015, doi: 10.1016/j.colsurfa.2015.05.008.
[38] R. W. Stevens, R. V. Siriwardane, and J. Logan, "In situ fourier transform infrared (FTIR) investigation of CO2 adsorption onto zeolite materials," *Energy and Fuels*, vol. 22, no. 5, pp. 3070–3079, 2008, doi: 10.1021/ef800209a.
[39] J. Tabačiarová, M. Mičušík, P. Fedorko, and M. Omastová, "Study of polypyrrole aging by XPS, FTIR and conductivity measurements," *Polym. Degrad. Stab.*, vol. 120, pp. 392–401, 2015, doi: 10.1016/j.polymdegradstab.2015.07.021.
[40] X. Du, Y. Xu, L. Xiong, Y. Bai, J. Zhu, and S. Mao, "Polyaniline with high crystallinity degree: Synthesis, structure, and electrochemical properties," *J. Appl. Polym. Sci.*, vol. 131, no. 19, pp. 6–13, 2014, doi: 10.1002/app.40827.
[41] I. Gawri, S. Khatta, K. P. Singh, and S. K. Tripathi, "Synthesis and characterization of polyaniline as emeraldine salt," *AIP Conf. Proc.*, vol. 1728, 2016, doi: 10.1063/1.4946338.
[42] P. Krishnamachari, R. Hashaikeh, and M. Tiner, "Modified cellulose morphologies and its composites; SEM and TEM analysis," *Micron*, vol. 42, no. 8, pp. 751–761, 2011, doi: 10.1016/j.micron.2011.05.001.
[43] Y. T. Ravikiran and B. Chethan, "Humidity sensing studies on conducting polymers: Polyaniline and polypyrrole," *Inorg. Chem. Commun.*, vol. 145, no. June, p. 110019, 2022,

doi: 10.1016/j.inoche.2022.110019.
[44] Y. F. Wang, D. L. Liu, J. J. Han, and A. R. Guo, "Detection of formaldehyde by cyclic voltammetry using a PANI/GO composite film–modified electrode," *Ionics (Kiel).*, vol. 28, no. 5, pp. 2457–2468, 2022, doi: 10.1007/s11581-022-04499-2.
[45] Q. Lu, W. J. Han, and H. J. Choi, "Smart and functional conducting polymers: Application to electrorheological fluids," *Molecules*, vol. 23, no. 11, 2018, doi: 10.3390/molecules23112854.
[46] X. Li, J. Meng, Y. Guo, X. Li, M. Li, and D. Gao, "Preparation and performance of polypyrrole modified filter paper humidity sensor by in situ polymerization," *Text. Res. J.*, vol. 93, no. 5–6, pp. 1389–1400, 2023, doi: 10.1177/00405175221128022.
[47] M. Golabi, A. P. F. Turner, and E. W. H. Jager, "Tuning the Surface Properties of Polypyrrole Films for Modulating Bacterial Adhesion," *Macromol. Chem. Phys.*, vol. 217, no. 10, pp. 1128–1135, 2016, doi: 10.1002/macp.201500445.
[48] H. J. Kim, S. Roy, and J. W. Rhim, "Effects of various types of cellulose nanofibers on the physical properties of the CNF-based films," *J. Environ. Chem. Eng.*, vol. 9, no. 5, p. 106043, 2021, doi: 10.1016/j.jece.2021.106043.
[49] V. S. Jamadade, D. S. Dhawale, and C. D. Lokhande, "Studies on electrosynthesized leucoemeraldine, emeraldine and pernigraniline forms of polyaniline films and their supercapacitive behavior," *Synth. Met.*, vol. 160, no. 9–10, pp. 955–960, 2010, doi: 10.1016/j.synthmet.2010.02.007.
[50] M. Parit, H. Du, X. Zhang, C. Prather, M. Adams, and Z. Jiang, "Polypyrrole and cellulose nanofiber based composite films with improved physical and electrical properties for electromagnetic shielding applications," *Carbohydr. Polym.*, vol. 240, no. December 2019, p. 116304, 2020, doi: 10.1016/j.carbpol.2020.116304.
[51] A. K. Rana, F. Scarpa, and V. K. Thakur, "Cellulose/polyaniline hybrid nanocomposites: Design, fabrication, and emerging multidimensional applications," *Ind. Crops Prod.*, vol. 187, no. PA, p. 115356, 2022, doi: 10.1016/j.indcrop.2022.115356.
[52] P. Bober *et al.*, "Biocomposites of Nanofibrillated cellulose, polypyrrole, and silver nanoparticles with electroconductive and antimicrobial properties," *Biomacromolecules*, vol. 15, no. 10, pp. 3655–3663, 2014, doi: 10.1021/bm500939x.
[53] S. Kotresh, Y. T. Ravikiran, H. G. Raj Prakash, C. V. V. Ramana, S. C. Vijayakumari, and S. Thomas, "Humidity sensing performance of spin coated polyaniline–carboxymethyl cellulose composite at room temperature," *Cellulose*, vol. 23, no. 5, pp. 3177–3186, 2016, doi: 10.1007/s10570-016-1035-6.
[54] R. Qi *et al.*, "Humidity sensors based on MCM-41/polypyrrole hybrid film via in-situ polymerization," *Sensors Actuators, B Chem.*, vol. 277, no. April, pp. 584–590, 2018, doi: 10.1016/j.snb.2018.09.062.
[55] I. Ragazzini *et al.*, "A resistive sensor for humidity detection based on cellulose/polyaniline," *RSC Adv.*, vol. 12, no. 43, pp. 28217–28226, 2022, doi: 10.1039/d2ra03982f.
[56] S. K. Mahadeva, S. Yun, and J. Kim, "Flexible humidity and temperature sensor based on cellulose-polypyrrole nanocomposite," *Sensors Actuators, A Phys.*, vol. 165, no. 2, pp. 194–199, 2011, doi: 10.1016/j.sna.2010.10.018.
[57] W. Zhang, L. Zhong, T. Wang, Z. Jiang, X. Gao, and L. Zhang, "Surface modification of cellulose nanofibers and their effects on the morphology and properties of polysulfone

membranes," *IOP Conf. Ser. Mater. Sci. Eng.*, vol. 397, no. 1, 2018, doi: 10.1088/1757-899X/397/1/012016.

A | Paper-based Devices Fabrication

This device has paper as substrate, a functional layer with the inks used for self-standing substrate fabrication and an interdigitated electrode to convert the chemical changes into an electrical signal. The different papers used as substrate include office paper, Whatman paper grade 1 and recycled paper (100, 80 and 50 g/cm^2) in 2.0 x 1.8 cm dimensions for each device. In these samples, the electrodes are screen printed with the same design and mesh as the other type of device, with silver and carbon ink. For the sensing layer, a tape mask is placed on the interconnects and the functional ink is deposited by doctor blade technique similarly to the other device, but the rod used has 6 µm and the tape height is 1065 µm.

B | Fabrication Process Schematic

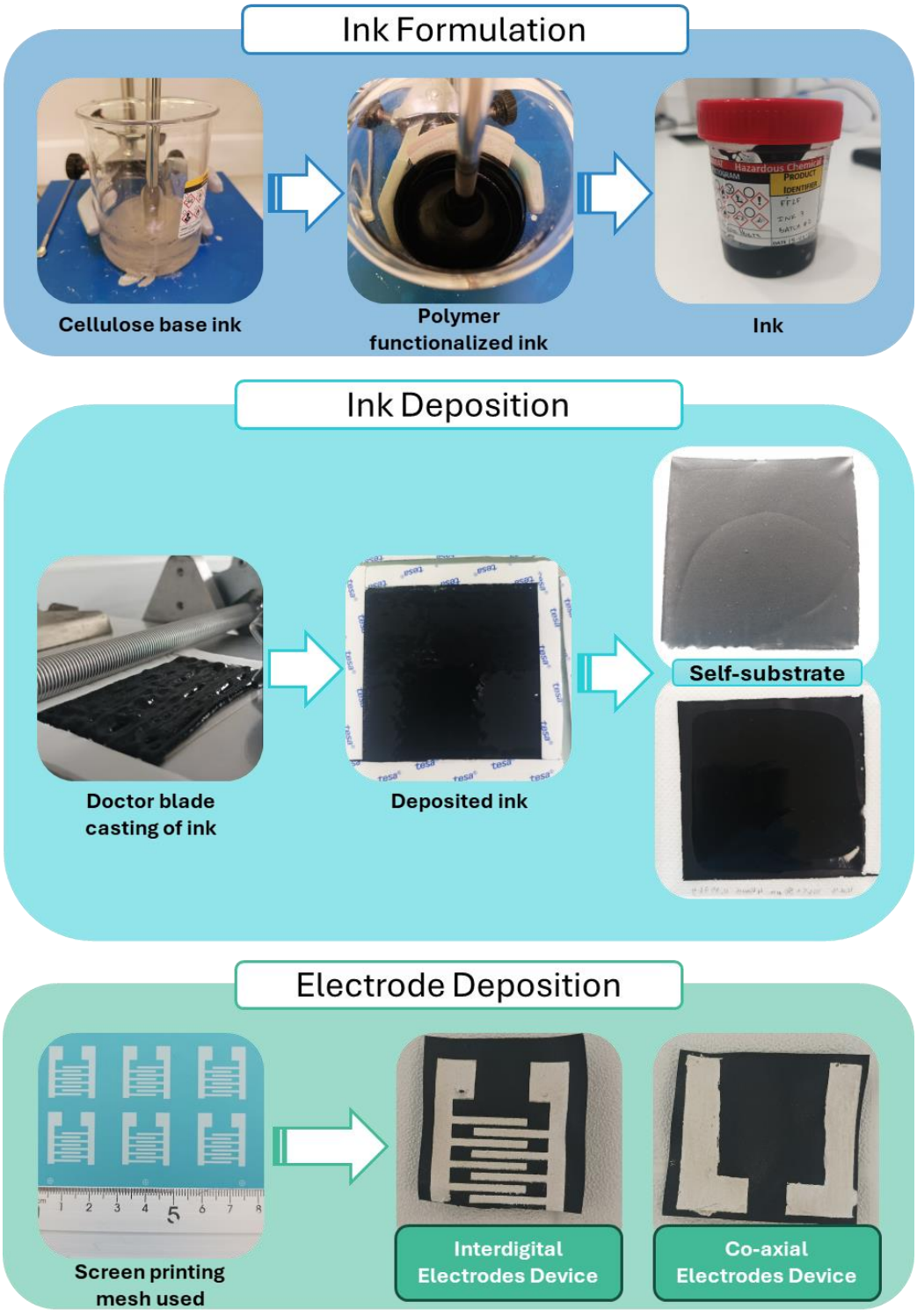

Figure 21 - Schematic of the fabrication process for self-standing substrates-based devices.

C | MATERIALS

For the polymer synthesis, the following reagents were used: Aniline (CAS No. 62-53-3, ≥99.5% purity, Sigma-Aldrich), Pyrrole (CAS No. 109-97-7, 98% purity, Sigma-Aldrich), Ammonium peroxodisulphate (APS, CAS No. 7727-54-0, PanReac AppliChem), Camphor-10-sulfonic acid (β) (CSA, CAS No. 5872-08-2, Sigma-Aldrich), Hydrochlorid acid fuming 37% (HCl 37%, CAS No. 7647-01-0, Merck), Ethanol absolute (CAS No. 64-17-5, Carlo Erba), Methanol (CAS No. 67-56-1, ≥99.8% concentration, Honeywell Riedel-de Haën™). To filter the powder Whatman Grade 1 Qualitative Filter Paper, GE Healthcare, Grade 1 Qualitative Filter Paper Standard Grade, sheet, 460 × 570 mm, Dimensions=460 x 570 mm (18.11 x 22.45) was used.

For ink production, sodium carboxymethyl cellulose (average Mw ~250,000, degree of substitution 0.7, CAS No. 9004-32-4, Sigma-Aldrich), cellulose nanofiber (Cellulose Nanofibril, Nanofibrillated Cellulose, CNFs, PowderNano), microfibrillated cellulose (3% MFC content, Celova® M150R-G, Weidmann), and sodium chloride (NaCl, CAS No. 7647-14-5, PanReac AppiChem) were used.

For electrode deposition, the inks were Saral SilverH2O 600 Silver Based Conductive Ink, Saralon and CRSN2664 C INK, Sun Chemical.

D | CHARACTERIZATION

The rheological behavior of the formulated inks was analyzed with Anton Paar MCR 502 rheometer and parallel plates geometry with a diameter of 25 mm.

For the compositional analysis of the self-standing substrates, 2 cm X 2 cm samples were analyzed using Raman spectroscopy (Renishaw Qontor InVia Raman microscope) and attenuated total reflectance Fourier transform infrared spectroscopy (ATR-FTIR, Nicolet™ Summit FTIR Spectrometer with an Everest™ Diamond ATR Accessory), covering a spectral range of 400 to 4000 cm^{-1}.

The morphology of the self-standing substrates was examined with an Ultra-high Resolution Scanning Electron Microscope (SEM-FIB, Hitachi SEM Regulus8220). Due to the low conductivity of the samples, they were coated with a thin gold layer.

Tensile tests were conducted on 3 cm x 1 cm self-standing substrate samples and paper samples (standard office paper and Whatman™ Chromatography Paper, Grade: 1CHR) using a Shimadzu EZ-Lx 10N Compact Table-Top Universal/Tensile Tester, operating at a speed of 50 mm/min. A minimum of four trials were performed for each sample.

For electrical measurements, 2 cm x 2 cm samples were connected using toothless flat alligator copper clips to a Keysight B2902B Precision Source/Measure Unit, from which the resistance values were extracted through I-V Sweep data.

To assess the hydrophilicity and wettability of the self-standing substrates, contact angle measurements were taken by sessile drop with 1 µL droplets of deionized water in a Dataphysics OCA15plus, and stability tests were conducted by dropping 1, 0.5, 0.25, and 0.1 mL of deionized water on 2 cm x 2 cm samples.

For humidity sensing, the sensor was placed inside a Weiss Technik Climate Cabinet TensileEvent CC/55/60/25O while connected to a Keysight B2902B Precision Source/Measure Unit to record electrical measurements. Each sample underwent one cycle from 10% to 60% relative humidity at 25°C. The circuit setup involved a voltage divider, with the Keithley providing 5 V and a resistance of 10kΩ, 11 kΩ or 10 MΩ.

For pressure sensing, the sensors were tested using finger pressure and balance scale weights of 100 g. The circuit consisted of a voltage divider, where an Arduino unit supplied a 5 V input, with resistances of 1 MΩ, 500kΩ, 100kΩ and 10kΩ.

E | *IN-SITU* POLYMERIZATION OF INKS

For the polymerization, the same process as the powder synthesis was followed with the substitution of water with the ink prepared. Due to the viscosity of the ink, mechanical stirring replaced magnetic stirring.

The 90mL volume of ink 11 is divided into two beakers into 30 and 60 mL. The set amounts of APS, HCl and PPy are added and stirred by hand and mechanically. Next, the beakers are transferred to the ice bath. When the temperature reaches 0-5ºC, the oxidant solution is transferred to the monomer solutions beaker and stirred by hand. However, due to the lower temperature, the inks viscosity was higher, and the mixing was not homogeneous, visible by the color change of the ink to black. Mechanically stirring revealed to be unsuited, as the ink became even more viscous due to the further polymerization of the cellulose, generating a gel like structure. Another issue lies with removing the unreacted reagents, since the films could not be dipped into a solvent without being destroyed.

F | ATR-FTIR Analysis

Table 5 - Summary of ATR-FTIR spectra analysis of self-standing substrates 7, 8, 14 and 15.

S-S 7	S-S 8	S-S 15	S-S 14	Assignment	Reference
3349	3335	3335	3362	O–H stretching (CMC, CNF, H_2O) N–H stretching (PPy, PANi)	[32]–[35]
2874	2868	2870	2879	C–H stretching (CMC, CNF)	[33], [34], [36], [37]
-	2360	2360	2360	CO_2 absorption	[38]
-	-	-	1725	C=O stretching (CMC)	[35]
1584	1580	1584	1587	C=C and C–N stretching of aromatic rings (PPy, PANi)	[34], [39]
1411	1413	1411	1413	$C–N^+$ stretching (PANi) C–H bending	[34], [40], [57]
-	-	1372	-	C–H bending vibrations	[35]
1317	1314	1316	1320	C–H, C–O aromatic rings vibrations	[36]
-	-	-	1267	C–H, C–N in-plane deformation C–N stretching in aromatic rings	[37], [41]
1203	1201	-	-	C–N stretching Breathing vibration of Py rings	[39], [41]
1152	1158	1154	-	C–OH stretching vibrations C–N in and out of plane deformation (PPy) C–O–C asymmetric stretching vibrations of β glycosidic linkage	[33], [34], [39]
1104	1095	1095	1104	C–O stretching	[35]
1022	1027	1020	1020	C–C, O–H stretching C–H deformation vibration (PPy)	[34], [36], [39], [41]
892	893	892	897	C–H aromatic out of plane bending of aromatic rings (PPy, PANi)	[34], [37]
783	779	-	-	C–H stretching	[37], [39]

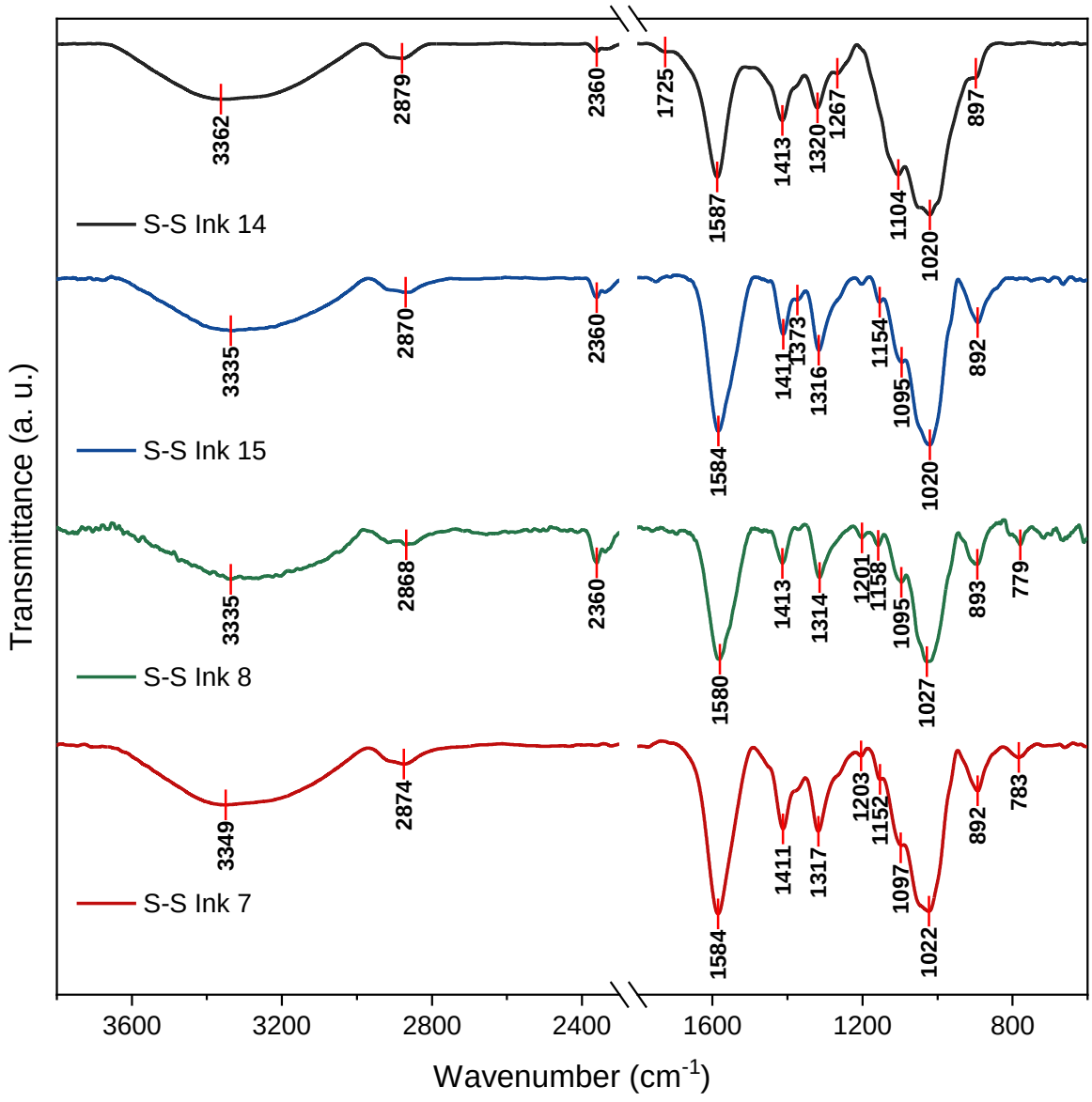

Figure 22 - ATR-FTIR spectra for self-standing substrates 7 (red), 8 (green), 14 (black), 15 (blue).

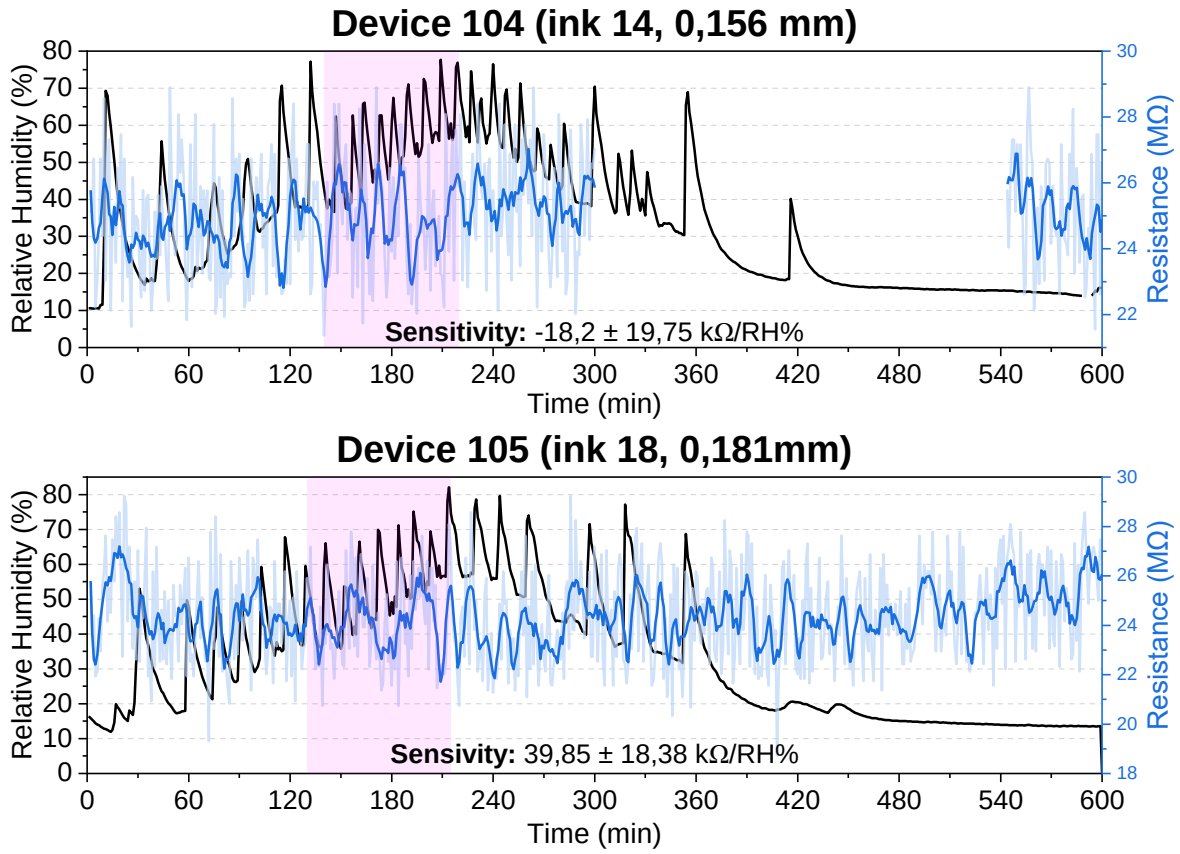

Figure 23 - Humidity sensing results of devices 104 and 105 in a 10 to 60 RH% cycle. In light blue is the real measurement of resistance while in dark blue is a smoothed curve to help understand the tendency of the data. The area in pink is the data used to measure the sensitivity of the sensor.

For device 104, the only containing PANi, the lack of accuracy to the proposed cycle makes the stabilizing sections at 20, 40 and 60 RH% unnoticeable and a peak at around 70 RH% is registered in the first half hour, exposing the device to higher humidity than wanted. A large portion of data was lost due to complications with the program, and it was not possible to repeat the test. The sensitivity in the 35 to 60 RH% range is negative, indicating that the overall tendency is decreasing with the increase of RH, the opposite of the expected behavior. To have more insight on the response to humidity of these self-standing substrates, this test should be repeated, as the present results have been affected by many variables.

Device 105 includes a small amount of NaCl (2.7%wt. of ink) to subside the oversaturation of the devices. This formulation was conceived very late into the thesis work, making it impossible to characterize the inks and self-standing substrates as other discussed

formulations. The resistance values are similar to other devices, so the addition of salt did not have a substantial effect on the conductivity of the self-standing substrate. In the first 30 minutes of the cycle, the sensitivity seems to have increased, yet this does not reflect in the remaining time, as there is a lot of variability in the results, the sensitivity in the 40 to 60 RH% range is approximate to device 33 in order of magnitude. However, it shows the same issue in the down cycle, as resistance keeps rising, indicating oversaturation. Increasing the amount of salt or experimenting with other salts are possible actions for improvement, but a study of the interaction with the remaining components of the composite film would be helpful to understand the issue further.

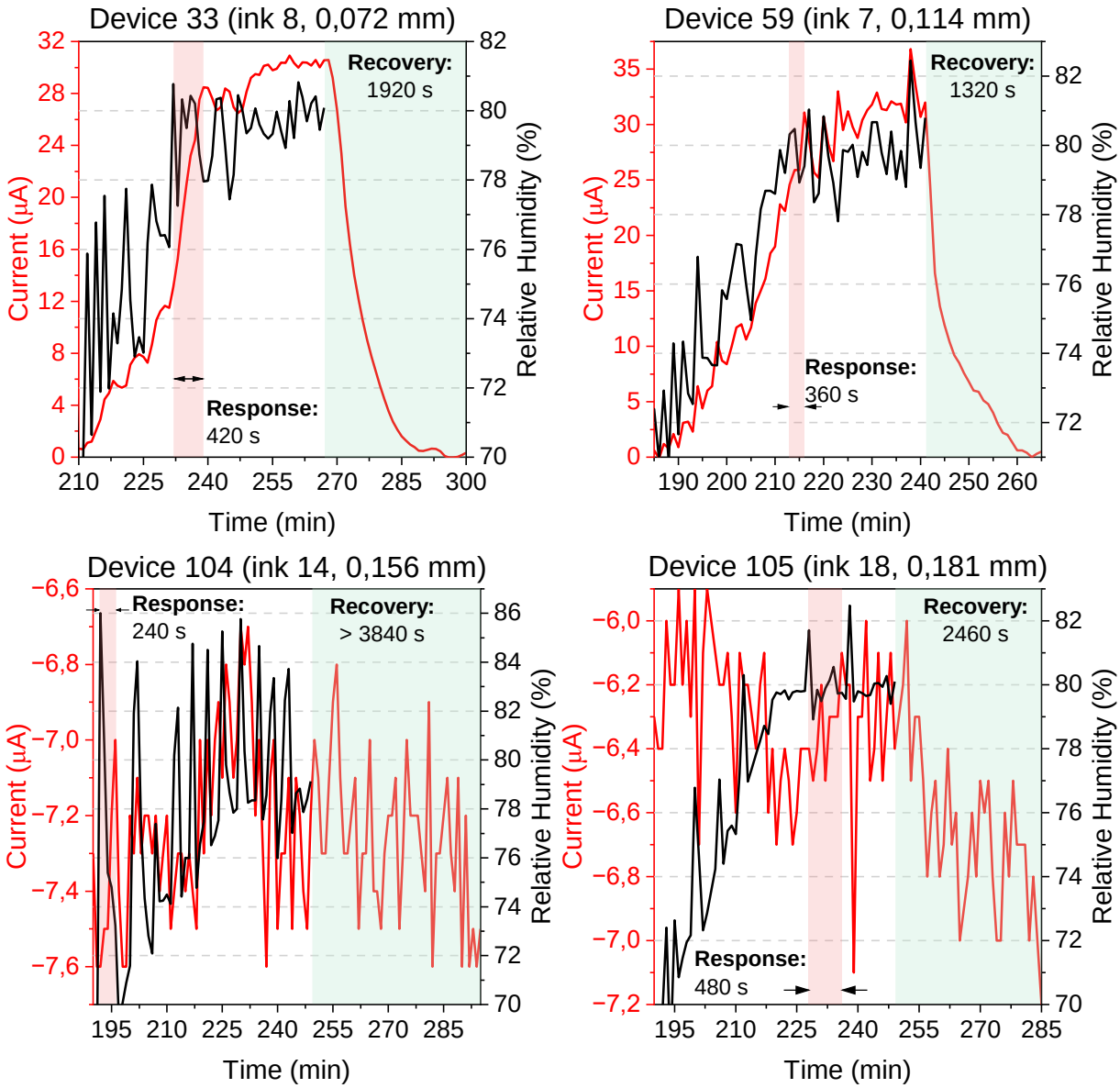

Figure 24 - Current response from 80 RH% of sensors with response (red area) and recovery (green area) times.

H | Pressure Sensing Testing Set-Up

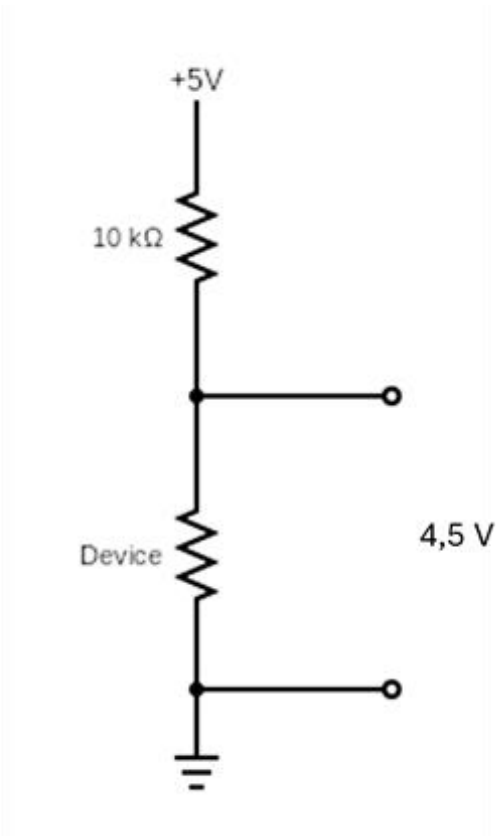

Figure 25 - Testing set-up for pressure sensing.